Bulk or surface grafted silylated Ru(ii) complexes on silica as luminescent nanomaterials

Sandra Cousinié, Léïla Mauline, Marie Gressier, Srinivasa Rao Kandibanda, Lucien Datas, Christian Reber, Marie-Joëlle Menu

Bulk or surface grafted silylated Ru(II) complexes on silica as luminescent nanomaterials

Sandra Cousinié,[a] Léïla Mauline,[a] Marie Gressier,[a] Srinivasa Rao Kandibanda,[a] Lucien Datas,[a] Christian Reber[b] and Marie-Joëlle Menu*[a]

DOI: 10.1039/c2nj21042h

A series of Ru(II) complexes with monosilylated-dipyridine ligand have been synthesized and fully characterized and were then covalently attached to silica nanoparticles. Two types of hybrids were obtained depending on the experimental procedure. In the first approach, metal complexes were incorporated inside the silica nanoparticles leaving a free hydroxylated silica surface for further functionalization. These silica based nanohybrids are similar to the well known nanoparticles encapsulating $[Ru(bpy)_3]^{2+}$ complexes preventing the release of the dye when used in aqueous or organic solutions. Size and luminescence properties vary throughout the series of metal complexes. The second approach leads to ruthenium(II) complexes covalently attached to the silica nanoparticle surface *via* hydrolysis and condensation of the ethoxysilyl group with silanol sites of Ludox type silica nanoparticles. This leads to the grafting of a monolayer for complexes with the monoethoxysilyl dipyridine ligand. In contrast, the complexes with triethoxysilyl ligands can lead to small amounts of oligomers, but their quantity is limited by the sterical constraints imposed by the molecular structure. The size of the hybrids depends on the starting particles. ^{29}Si and ^{13}C solid state NMR are used to characterize silica surface properties whereas TEM and SEM confirm nanosize and morphology of the hybrids. The complexes and the nanohybrids are luminescent, with variations for ruthenium(II) complexes that are covalently incorporated or grafted on the silica surface.

1. Introduction

The encapsulation of transition metal complexes in silica nanoparticles has been the focus of considerable attention over the past decade, since they can act as redox,[1,2] magnetic[3,4] or optical[5,6] nanoprobes for biotechnology applications. Among dye doped silica nanoparticles, tris(2,2′-dipyridyl)ruthenium(II) chloride is one of the most popular luminophores and extensively applied in bioanalysis and biodetection[7–10] as a result of the good chemical stability and high luminescence quantum yield.[11,12] Very few monosubstituted dipyridyl derivatives are reported for ruthenium(II). One example was synthesized by Schubert and co-workers, isolating methylmethacrylate-containing bipyridine monomers[13] (Scheme 1a–i) which give rise to new materials for polymer solar cells through polymerisation and ruthenium(II) complexation reactions. The methylmethacrylate group as an anchoring function is only interesting for the PMMA organic polymer matrix, but dicarboxylato-dipyridine[14] (Scheme 1a–ii) was largely used in photoelectrolysis and electrocatalysis using tin or titanium dioxide as inorganic matrices. Nevertheless, interactions with the silica surface are much smaller than siloxane bonds, illustrating the need for silylated derivatives such as disubstituted dipyridine (Scheme 1a–iii) which have been recently isolated by Monnier *et al.*[15] In previous work we have reported the synthesis of monosilylated 2,2′-dipyridine (**1** and **2** Scheme 1a) with the aim to elaborate new nanostructured hybrid materials[16] such as new efficient luminescent materials. In this research field two synthetic routes have been explored depending on whether silylated metal complexes are isolated and purified or not, and in the latter case hybrid materials are obtained using a procedure with at least two steps.

In Scheme 1b we illustrate the dipyridine complexes bearing silane functions such as trichlorosilane[17] (**A**), triethoxysilane[18] (**B**) or dimethylethoxysilane[19] (**C**). Complexes **A** and **C** are interesting because of the presence of only one organosilane function which allows us to control hydrolysis and condensation reactions during the synthesis of hybrid materials. This also improves the purity of the hybrids by inhibiting the oligomerisation of the monomers, in particular for the monoethoxysilylated complex (**C**). In the last part of Scheme 1 (**D–I** hybrids), we illustrate rare examples of hybrid materials bearing monosilylated dipyridine metal complexes

[a] *Université de Toulouse, UPS, Centre Interuniversitaire de Recherche et d'Ingénierie des Matériaux, UMR-CNRS 5085, Université Paul Sabatier, 118 route de Narbonne, 31062 Toulouse Cedex 9, France. E-mail: menu@chimie.ups-tlse.fr; Fax: +33 561556163, +33 5 61558487*
[b] *Département de Chimie, Université de Montréal, Montréal QC H3C3J7, Canada. E-mail: christian.reber@umontreal.ca; Tel: +1 514 340-4711*

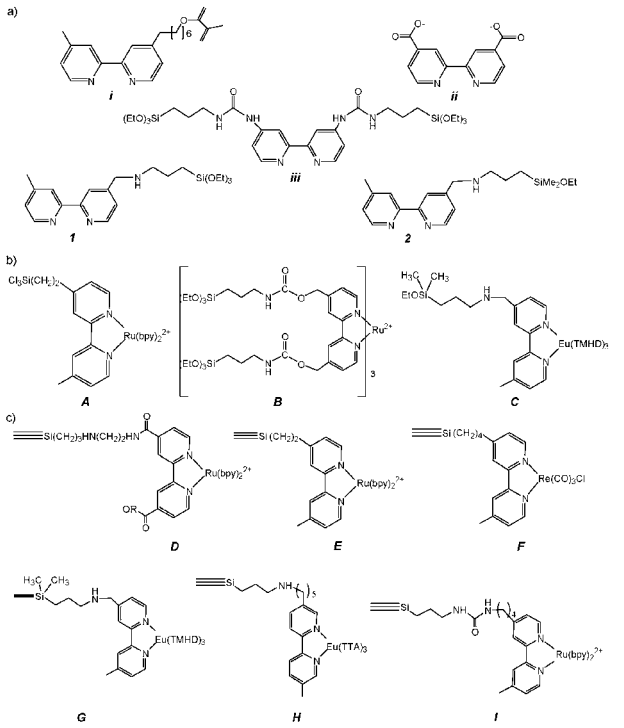

Scheme 1 Precursors and hybrids: (a) dipyridine molecules containing both anchoring and complexing functions; (b) silylated-dipyridine complexes; (c) related metallated hybrid materials.

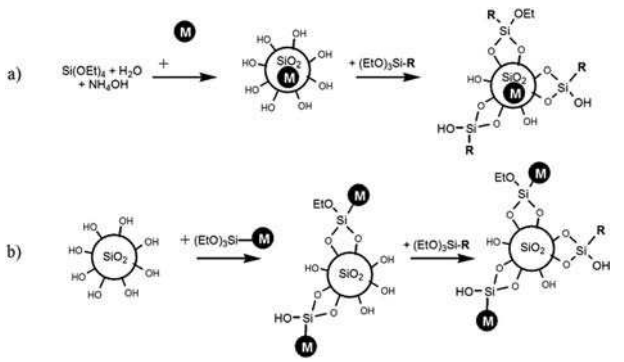

Scheme 2 Synthetic routes for bifunctional metallated nanohybrids: (a) dye incorporation and surface functionalization by organosilane grafting; (b) dye containing organosilane ligand is grafted on the silica nanoparticle surface.

(Ru(II), **D–E**, **I**; Re(I), **F** and Eu(III), **G–H**). The versatility of this chemistry is well illustrated by these hybrids with different metal centers, differently silylated dipyridine ligands, and different chemical nature and morphology of the oxide matrices, leading to a promising area for new applications.[1–6] **D** and **E** are tin dioxide based hybrids implying both a bulky matrix synthesized in a three-step procedure for **D**, whereas a direct condensation reaction of chlorosilylated complex **A** is used to obtain **E**.[14] **F–I** are silica based hybrids, **F**[20] and **H**[21] are obtained by complexation reactions on the modified silica surface on quartz plates and silicon wafers, respectively, whereas silica nanoparticle surfaces were directly functionalized by the reaction of the silylated europium(III) complex, **C**, with colloidal silica nanoparticles leading to metallated hybrid **G**.[19] In the latter case, monolayered chemical modification has been obtained due to the monoethoxysilane anchoring function of the dipyridine ligand **2**. Surprisingly, monosilylated dipyridine ruthenium(II) complexes have rarely been used to prepare luminescent silica based nanoparticles. At our knowledge only one example, **I**, of covalent incorporation on silica nanoparticles has been recently reported by Zanarini *et al.*[22] The main synthetic goal of our work is the development of both bulk and surface grafted nanomaterials. So we have isolated new ruthenium(II) complexes related to $[Ru(bipy)_3]Cl_2$ containing monosilylated dipyridine ligand bearing triethoxysilane, **1**, and monoethoxysilane, **2** (Scheme 1a). They are then incorporated in silica nanoparticles using the water-in-oil microemulsion method. We also document the luminescence properties of these materials. In both approaches, the interaction between dye and the silica matrix is through siloxane bond formation, leading to class II hybrid materials, in contrast to class I materials, where electrostatic interactions dominate.[23]

The first goal of our work is the immobilization of the dye molecule in order to prevent the leaching and bleaching effects reported for class I systems, an advantage of the class II hybrid materials described recently by Carbonaro *et al.*[24] explored as candidates for solid-state laser applications. These authors have immobilized an organic dye, rhodamine 6G, using isocyanatopropylsilane as the coupling agent between dye and silane precursor for silica. Bifunctional silica nanoparticles can be obtained when luminescent silica nanoparticles incorporating the dye are modified by grafting of organosilylated ligands, as illustrated in Scheme 2a.

Another approach consists in grafting of transition metal complexes on the silica surface, illustrated in Scheme 2b. These complexes can potentially provide further reactivity depending on the coordination sphere of the metal centre and the residual silanol of the silica surface (Scheme 2b). Grafting of silylated complexes can also give rise to multifunctional core–shell magnetic silica nanocomposites as shown by Zu *et al.*[25] They grafted a silylated phenanthroline ruthenium(II) complex on Fe_3O_4 cores coated with a silica shell, resulting in a covalently attached luminescent ruthenium(II) complex. This system can be further encapsulated by an additional silica shell and is an example of a multifunctional nanocomposite with magnetic, luminescent and electro-chemiluminescent properties, emphasizing the versatility of silica based nanomaterials, and a starting point for further development in this research field.

Direct grafting of silylated complexes on the silica surface leads to metallated sites with their own coordination properties giving rise to applications of these new materials in catalysis, as chemical sensors or luminescent probes as described previously[19] for silylated lanthanide complexes. We have shown that direct grafting of the organosilylated metal complexes is preferred over the complexation reaction of the metal ions or chelates on organically modified silica surfaces to obtain homogeneous functionalized silica materials.[18] The silylated dipyridine ligands (**1** and **2** in Scheme 1a) were used to synthesize ruthenium(II) complexes similar to tris(2,2′-dipyridine) ruthenium(II) chloride, with the triethoxy- or monoethoxy-silylated dipyridine ligands used as attaching moieties. The cationic or neutral complexes contain at least one organosilyldipyridine ligand and other unsubstituted dipyridine ligands in order to obtain an intense

ligand to metal charge transfer transition (MLCT). All these complexes are new luminophores and have been incorporated or grafted according to the first step of the reactions in Scheme 2a and b. Grafting and incorporation reactions have been studied and the luminescence properties for each metallated hybrid have been evaluated.

2. Experimental section

2.1 Materials

Ludox AS40 (40 wt% SiO_2, 23 ± 2 nm, pH = 9) and tetraethoxysilane (TEOS; 99 999%) obtained from Aldrich were used as starting silica materials. Ethanol, hexan-1-ol, ammonia (32%) and Triton X-100 used as a surfactant were purchased from ACROS. Silver tetrafluoroborate $AgBF_4$ (99%) and dipyridine (>99%) were purchased from Aldrich. The silylating agents, 4-methyl-4′-[methylamino-3(propyltriethoxy-silyl)]-2,2′-dipyridine, **1**, and 4-methyl-4′-[methylamino-3(propyldimethyl-ethoxy-silyl)]-2,2′-dipyridine, **2**, were synthesized as previously described by Menu and co-workers[16] and characterized by UV, IR, MS, ^{13}C, ^{1}H, ^{29}Si NMR spectroscopies.[26] $RuCl_2(bpy)_2$ (bpy = dipyridine), $RuCl_2(DMSO)_4$ (DMSO = dimethylsulfoxide), $RuCl_3(tpy)$ (tpy = 2,2′:6′,2″-terpyridine) and $[Ru(bpy)_3]Cl_2$ (as reference) were synthesized as previously described[27–30] with 85%, 96%, 95% and 85% yields, respectively. Pentane, diethylether, dichloromethane and ethanol were purified by distillation before use. All experiments concerning the preparation of the ligands and the complexes were performed under an inert atmosphere using the Schlenk tube technique. Solvents are degassed before using cryogenic procedures.

2.2 Characterization

We have characterized the ruthenium complexes by infrared spectroscopy in the range of 4000–400 cm^{-1} with a Bruker Vector 22 spectrophotometer and infrared spectra of the functionalized silica nanoparticles were obtained with the diffuse reflectance technique with a Perkin-Elmer 1760 X with DTGS detector. Mass spectra were recorded by FAB or IS technique using a Nermag R10-10 spectrometer or a TSQ 7000 Thermo-Quest Spectrometer. UV-VIS absorption spectra in the range of 900–200 nm, 1 cm optical path, were recorded using a Varian Cary 1E spectrometer. C, H, N elemental analyses were performed on a Carlo Erba EA 1110 instrument. Simultaneous thermogravimetric (TG) and differential thermal (DT) analyses were carried out on a SETARAM TG-DTA 92 thermobalance using 20 mg of sample; α-alumina was used as the reference. The heating rate was 3.8 °C min^{-1}. The temperature range was 20–1200 °C and the analyses were done using a 1.5 L h^{-1} air flow. The amount of grafted or incorporated material, τ, in mmol per gram of silica, was determined by two methods. The first estimate is calculated from the nitrogen content according to the formula $\tau = \%N \times 10^3/(14 \times 100 \times n_N)$, where %N and n_N represent the nitrogen content in percent and the number of nitrogen atoms in the grafted or incorporated moiety, respectively. The second estimate of the grafted or incorporated amount is obtained by DTA/DTG measurements with the formula $\tau = \Delta m_2 \times 10^3/(m \times M)$, with Δm_2 representing the weight loss in the temperature range 200–500 °C, m the sample amount and M the molecular mass of the grafted or incorporated moiety. ^{1}H and $^{13}C\{^{1}H\}$ NMR spectra of molecular derivatives in solution ($CDCl_3$, MeOD, DMSO-D_6, CD_3CN, acetone-D_6) were measured using Bruker Avance 300 (300.180 MHz, 75.468 MHz and 59.63 MHz for ^{1}H, ^{13}C and ^{29}Si respectively). Chemical shift (δ) is given in ppm, relative to solvent signal; signal multiplicity is noted as s = singlet, d = doublet, t = triplet, q = quadruplet, m = multiplet. Coupling constant (J) are expressed in Hz. ^{1}H decoupled ^{29}Si MAS (Magic Angle Spinning) Nuclear Magnetic Resonance (NMR) spectra of silica based hybrids were recorded on a Bruker Avance II 400 WB spectrometer. ^{1}H–^{29}Si and ^{1}H–^{13}C CP MAS NMR experiments were also performed in natural abundance at frequencies of 79.391 and 100.356 MHz for silicon and carbon, respectively. Decompositions of the NMR spectra to extract the proportion of the corresponding species were performed with the DMfit software.[31] Transmission electron microscopy (TEM) was used to determine morphology and particle size. FEG-SEM observations of hybrid nanomaterials were done on a JEOL JSM 6700 F operating at 15 kV. TEM analyses were carried out on a JEOL 2010 (200 kV). A drop of sol was diluted in ethanol. Then a carbon-coated grid was dipped in the solution and allowed to dry at room temperature. Luminescence spectra were recorded with a Renishaw Invia microscope spectrometer using the 488 nm line of an argon ion laser as the excitation source. The spectral resolution of the instrument is 0.02 nm. The sample temperature was controlled with nitrogen gas and a Linkam microscope cryostat.

2.3 Synthesis

2.3.1 Synthesis of ruthenium(II) complexes containing 4-methyl-4′-[methylamino-3(propylalkoxysilyl)]-2,2′-dipyridine

*$[Ru(bpy)_2(\mathbf{1})]X_2$, X = BF_4 (**3**), Cl (**3′**) and $[Ru(bpy)_2(\mathbf{2})]X_2$, X = BF_4 (**4**), Cl (**4′**) starting with $RuCl_2(bpy)_2$.* Dichloridebis-(dipyridine)ruthenium(II), 262 mg (0.5 mmol) and 195 mg (1 mmol) of silver tetrafluoroborate dissolved in 50 mL of deoxygenated acetone and were refluxed for 4 hours. The solution was filtered to eliminate silver chloride and transferred on 302 mg (0.75 mmol) of **1**. The resulting mixture was refluxed for 3 hours. The solution was concentrated to half and diethylether (75 mL) was added. After precipitation, the solid was filtered and dried under vacuum. 485 mg (4.9 mmol) of an orange brown powder of **3** were isolated with 98% yield. The same reaction using **2** (256 mg, 0.75 mmol) as the silylated dipyridine ligand gives **4** as brown powder (330 mg) with 71% yield.

Briefly for **3′**, **1** (180 mg, 0.44 mmol) was added to a solution of *cis*-$RuCl_2(bpy)_2{\cdot}2H_2O$ (200 mg, 0.38 mmol) in dry ethanol (50 mL). The mixture was allowed to reflux for 24 h. After the removal of half of the solvent, the complex was precipitated by adding chloroform and diethyl ether to obtain **3′** in 82% yield.

$[Ru(bpy)_2(\mathbf{1})](BF_4)_2$, **3**: EA found C, 49.2; H, 4.95; N, 9.9. Calc. for $C_{41}H_{49}B_2N_7O_3F_8RuSi$: C, 49.7; H, 5.0; N, 9.9. UV $\lambda_{max}(CH_2Cl_2)$/nm 254 (ε dm^3 mol^{-1} cm^{-1} 45 996), 290 (96 920), 426 (7732), 458 (10 670). IR ν, δ/cm^{-1} 2927 $\nu_{as}(CH_2, CH_3)$; 1617 ν(CN); 1598, 1559 $\nu(CC)_{bipy'}$; 1464, 1445, 1422 $\nu(CC)_{bipy}$; 1377 $\delta(CH_2)$; 1058 $\nu(BF_4)$; 768 $\delta(CH_{Ar})$.

$[Ru(bpy)_2(\mathbf{1})]Cl_2{\cdot}2H_2O$ **3′**: EA found C, 51.3; H, 5.8; N, 10.1. Calc. for $C_{41}H_{49}N_7O_3Cl_2SiRu{\cdot}2H_2O$: C, 53.3; H, 5.8; N, 10.6%. UV $\lambda_{max}(H_2O)$/nm 287 (ε dm^3 mol^{-1} cm^{-1} 59 330),

456 (10 145). IR ν, δ/cm^{-1} 3400 ν(OH_{water}); (3066 ν(CH_{ar}); 2971 ν_{as}(CH_3); 2923 ν_{as}(CH_2); 2882 ν_s(CH_3); 1640 δ(HOH_{water}); (1638, 1617 ν(CN); 1599, 1463, 1444, 1420 ν(CC); 1380 δ(CH_2); 1240 ν(SiC); 1107, 1069br ν($SiOC_2H_5$); 957 δ(SiO); 768 δ(CH_{ar}). ^{1}H NMR δ_H(300.13 MHz; MeOD; ppm) 0.69 (2H, m, CH_2, 11-H); 1.20 (9H, t, J_{AB} = 6.9, CH_3, 13-H); 1.69 (2H, m, CH_2, 10-H); 2.60 (3H, s, CH_3, 7-H); 2.65 (2H, m, CH_2, 9-H); 3.55 (6H, q, J_{AB} = 6.9, CH_2, 12-H); 3.98 (2H, s, CH_2, 8-H); 7.34 (1H, d, J_{AB} = 5.7, CH, 5′-H); 7.50 (5H, m, CH, 5-H and V-H); 7.62 (1H, d, J_{AB} = 5.7, CH, 6′-H); 7.70 (1H, d, J = 5.7, CH, 6-H); 7.83 (4H, s, CH, IV-H); 8.13 (4H, m, CH, III-H); 8.61 (1H, s, CH, 3′-H); 8.72 (5H, m, CH, 3-H and VI-H). ^{13}C NMR δ_C(75.5 MHz; MeOD; ppm) 9.1 (1C, CH_2, 11); 18.6 (3C, CH_3, 13); 21.5 (1C, CH_3, 7); 24.2 (1C, CH_2, 10); 53.0 (1C, CH_2, 9); 53.5 (1C, CH_2, 8); 58.5 (3C, CH_2, 12); 125.1 (1C, CH, 3′); 125.9 (4C, CH, III); 126.7 (1C, CH, 3); 128.4 (1C, CH, 5′); 129.1 (2C, CH, V); 130.1 (1C, CH, 5); 139.3 (4C, CH, IV); 151.9 (1C, C, 4′); 152.4 (2C, CH, 6, 6′); 152.8 (4C, CH, VI); 154.0 (1C, C, 4)); 158.2 (1C, C, 2′); 158.5 (1C, C, 2); 158.8 (4C, C, II). MS (FAB) m/z 852 (M + H–HCl; 408, M−2Cl).

[Ru(bpy)$_2$(**2**)](BF$_4$)$_2$, **4**: EA found C, 49.1; H, 4.65; N, 9.9. Calc. for $C_{39}H_{45}B_2N_7OF_8RuSi$: C, 50.34; H, 4.9; N, 10.5%. UV λ_{max}(CH_2Cl_2)/nm 246 (ε dm^3 mol^{-1} cm^{-1} 74 856), 286 (78 617), 424 (8020), 453 (9648). IR ν, δ/cm^{-1} 2952 ν_{as}(CH_2, CH_3); 1619 ν(CN); 1602, 1556w, 1464, 1445, 1422 ν(CC)$_{bipy}$; 1250 ν(SiC); 1055 ν(BF_4); 769 δ(CH_{Ar}). ^{1}H NMR δ_H(300.13 MHz; MeOD; ppm) 0.06 (6H, m, CH_3, Si–Me); 0.54 (2H, l, CH_2, 11-H); 1.10 (3H, t, CH_3, 14-H); 1.62 (2H, l, CH_2, 10-H); 2.52 (3H, s, CH_3, 7-H); 2.74 (2H, l, CH_2, 9-H); 3.42 (2H, q, CH_2, 13-H); 4.04 (2H, l, CH_2, 8-H); 7.29 (1H, d, CH, 5′-H); 7.31 (1H, d, CH, 5-H); 7.45 (4H, t, CH, IV-H); 7.55 (1H, s, CH, 3′-H); 7.57 (1H, s, CH, 3-H); 7.65 (4H, d, CH, III-H); 8.08 (4H, t, CH, V-H); 8.58 (1H, l, CH, 6′-H); 8.66 (1H, l, CH, 6-H); 8.75 (4H, d, CH, VI-H). ^{13}C NMR δ_C(75.5 MHz; CD_3CN; ppm) 0.1 (2C, CH_3, Si–Me); 12.5 (1C, CH_2, 11); 19.8 (1C, CH_3, 14); 19.9 (1C, CH_3, 7); 22.1 (1C, CH_2, 10); 50.9 (1C, CH_2, 8); 51.7 (1C, CH_2, 9); 52.3 (1C, CH_2, 13); 124.1 (1C, CH, 3′); 124.9 (4C, CH, III); 126.0 (1C, CH, 3); 127.5 (1C, CH, 5′); 128.3 (4C, CH_3, V); 128.5 (1C, CH, 5); 137.7 (4C, CH, IV); 150.8 (1C, CH, 6′); 151.0 (2C, C, 4, 4′); 151.2 (1C, CH, 6); 151.3 (4C, CH, VI); 156.4 (1C, C, 2′); 157.1 (5C, C, II; 2). MS (IS) m/z 932 (M + H).

*RuCl$_2$(DMSO)$_2$(**1**), **5**, and RuCl$_2$(DMSO)$_2$(**2**), **6**, starting with RuCl$_2$(DMSO)$_4$.* Organosilyldipyridine ligand **1** (208 mg, 0.52 mmol) for complex **5** and **2** (179 mg, 0.52 mmol) for complex **6** were taken in 50 mL of dry ethanol separately under anaerobic conditions. 0.250 mg (0.52 mmol) of dichlorotetrakis-(dimethylsulfoxide)ruthenium(II), RuCl$_2$(DMSO)$_4$, was added to both solutions. The mixtures were refluxed for 2 hours. The solvent was completely evaporated, then 50 mL of dry acetone was added to dissolve the solid and the obtained solution was concentrated to half. Precipitation is obtained when dry diethylether (50 mL) was added. The brown solid is filtered and dried under vacuum giving 380 mg (0.28 mmol, 53% yield) of **5** or 216 mg (0.335 mmol, 60% yield) of **6**.

RuCl$_2$(DMSO)$_2$(**1**), **5**: EA found C, 39.2; H, 5.9; N, 6.2. Calc. for $C_{25}H_{45}N_3O_5S_2Cl_2RuSi$: C, 41.0; H, 6.2; N, 5.75%. UV λ_{max}(CH_2Cl_2)/nm 226 (ε dm^3 mol^{-1} cm^{-1} 21 465), 290 (24 601), 435 (2057). IR ν, δ/cm^{-1} 2922 ν_{as}(CH_2, CH_3); 1619 ν(CN); 1554 ν(CC)$_{bipy'}$; 1480 δ(NH); 1363 δ(CH_2); 1190 ν(SO_S); 1095br ν(SiOC); 969 δ(SiO); 718 ν_{as}(CS); 680 ν_s(CS); 427 δ(CSO). ^{13}C CP MAS NMR δ_C(100.5 MHz; ppm) 11.2 (1C, CH_2, 11); 21.6 (3C, CH_3, CH_3, CH_2, 14, 7, 10); 31.6 (2C, CH_2, 9, 8); 46.4 (4C, CH_3, DMSO); 58.5 (3C, CH_2, 13); 125.0 (4C, CH, 3′, 3, 5′, 5); 151.3 (4C, C, CH, 4′, 6, 6′, 4); 157.1 (2C, C, 2′, 2).

RuCl$_2$(DMSO)$_2$(**2**), **6**: EA found C, 41.6; H, 6.05; N, 6.4. Calc. for $C_{23}H_{41}N_3O_3S_2Cl_2RuSi$: C, 41.1; H, 6.15; N, 6.3%. UV λ_{max}(CH_2Cl_2)/nm 227 (ε dm^3 mol^{-1} cm^{-1} 20 447), 292 (23 099), 380 (5663). IR ν, δ/cm^{-1} 2920 ν_{as}(CH_2, CH_3); 1618 ν(CN); 1552 ν(CC)$_{bipy'}$; 1481 δ(NH); 1361 δ(CH_2); 1250 ν(SiC); 1179 ν(SO_S); 1073br ν(SiOC); 969 δ(SiO); 717 ν_{as}(CS); 681 ν_s(CS). ^{1}H NMR δ_H(300.13 MHz, DMSO-d$_6$; ppm) 0.00 (6H, m, CH_2, Si–Me); 0.44 (2H, m, CH_2, 11-H); 0.93 (3H, s, CH_3, 14-H); 1.55 (2H, m, CH_2, 10-H); 2.31 (3H, s, CH_3, 7-H); 2.55 (2H, m, CH_2, 9-H); 3.24 (3H, s, CH_3(DMSO)); 3.34 (6H, m, CH_3(DMSO)); 3.48 (3H, s, CH_3(DMSO)); 3.48 (2H, q, CH_2, 13-H); 3.86 (2H, s, CH_2, 8-H); 7.09 (1H, d, CH, 5′-H); 7.34 (1H, s, CH, 5-H); 8.17 (1H, s, 1H, CH, 3′-H); 8.30 (1H, s, CH, 3-H); 8.48 (1H, m, CH, 6′-H); 8.56 (1H, m, CH, 6-H). MS (IS) m/z 636 (M + H–HCl).

*RuCl$_2$(bpy)(**1**), **7** and RuCl$_2$(bpy)(**2**), **8**, starting with complexes **5** and **6** respectively.* 126 mg (0.81 mmol) of dipyridine was taken in dry ethanol (50 mL) under anaerobic conditions, to this solution 590 mg (0.81 mmol) of RuCl$_2$(DMSO)$_2$(**1**), and 544 mg (0.81 mmol) of RuCl$_2$(DMSO)$_2$(**2**) were added for the complexes **7** and **8** respectively. After two hours refluxing, the reaction mixture was concentrated to half and diethylether was added (50 mL) to precipitate the product. Solid was filtered and dried under vacuum to give 368 mg (0.50 mmol, yield: 62%) of **7** and 336 mg (0.50 mmol, yield: 62%) of **8**.

RuCl$_2$(bpy)(**1**), **7**: EA found C, 49.1; H, 5.8; N, 9.85. Calc. for $C_{31}H_{41}N_5O_3Cl_2RuSi$: C, 50.8; H, 5.65; N, 9.6%. UV λ_{max}(CH_2Cl_2)/nm 228 (ε dm^3 mol^{-1} cm^{-1} 8189), 290 (8637), 466 (1213). IR ν, δ/cm^{-1} 2924 ν_{as}(CH_2, CH_3); 1617 ν(CN); 1596 ν(CC)$_{bipy'}$; 1458, 1444, 1421 ν(CC)$_{bipy}$; 1074br ν(SiOC); 772 δ(CH_{Ar}). ^{13}C CP MAS NMR ^{13}C δ_C(100.5 MHz; ppm) 10.8 (1C, CH_2, 11); 21.4 (3C, CH_3, CH_3, CH_2, 14, 7, 10); 51.4 (2C, CH_2, 8, 9); 56.7 (1C, CH_2, 13); 125.6 (12C, CH, 3′,III, 3, 5′, V, 5); 138.8 (2C, CH, IV); 150.5 (12C, C, CH, 4′, 6, 6′, VI, 4); 156.7 (6C, C, 2′, 2, II). MS (IS) m/z 696 (M + H–HCl).

RuCl$_2$(bpy)(**2**), **8**: EA found C, 51.7; H, 5.85; N, 10.15. Calc. for $C_{29}H_{37}N_5OCl_2RuSi$: C, 51.85; H, 5.55; N, 10.4%. UV λ_{max}(CH_2Cl_2)/nm 240 (ε dm^3 mol^{-1} cm^{-1} 21 859), 288 (43 505), 424 (3067), 455 (4024). IR ν, δ/cm^{-1} 2952 ν_{as}(CH_2, CH_3); 1614 ν(CN); 1601 ν(CC)$_{bipy'}$; 1457, 1436, 1415 ν(CC)$_{bipy}$; 1254 ν(SiC); 1042br ν(SiOC); 769 δ(CH_{Ar}). MS (IS) m/z 694 (M + Na).

*[RuCl(tpy)(**1**)]Cl, **9** and [RuCl(tpy)(**2**)]Cl, **10** starting with RuCl$_3$(tpy).* Mixture of 194 mg (0.44 mmol) of trichloroterpyridine ruthenium(III) and 806 mg (2 mmol) of **1** and 686 mg (2 mmol) of **2** for complexes **9** and **10**, respectively, were taken in dry ethanol (70 mL) containing 0.675 mL (4.85 mmol) of triethylamine and refluxed for 4 hours under anaerobic conditions. Solvent was evaporated; complexes **9** and **10** were extracted with dichloromethane and precipitated after addition of diethylether (15 mL). Product was filtered and dried under vacuum to give 232 mg (0.29 mmol, 65% yield) of **9** and 194 mg (0.26 mmol, 59% yield) of **10**.

[RuCl(tpy)(**1**)]Cl, **9**: EA found C, 52.7; H, 5.8; N, 10.8. Calc. for $C_{36}H_{44}N_6O_3Cl_2RuSi$: C, 53.45; H, 5.5; N, 10.4%. UV λ_{max}(EtOH)/nm 239 (ε dm^3 mol^{-1} cm^{-1} 24 000), 284 (30 682), 318 (5955). IR ν, δ/cm^{-1} 2925 $\nu_{as}(CH_2, CH_3)$; 1654 ν(CN); 1616 $\nu(CC)_{tpy}$; 1598, 1559, 1458 $\nu(CC)_{bipy}$; 1379 $\delta(CH_2)$; 1246 ν(SiC); 1079br ν(SiOC); 997 δ(SiO); 773 $\delta(CH_{Ar})$. ^{13}C NMR δ_C(75.5 MHz; acetone-d$_6$; 208 K; ppm) 11.0 (1C, CH_2, 11); 18.2 (3C, CH_3, 13); 28.6 (1C, CH_2, 10); 30.9 (1C, CH_3, 7); 42.2 (1C, CH_2, 8); 56.6 (4C, CH_2, 9, 12); 117.5 (2C, CH, III′); 120.8 (4C, CH, III); 121.4 (2C, CH, V); 124.7 (2C, CH, 3′; 3); 125.2 (2C, CH, 5′, 5); 137.6 (2C, CH, IV); 138.7 (1C, CH, IV′); 149.2 (4C, CH, 4′, 6, 6′, 4); 149.5 (2C, CH, VI); 155.0 (2C, CH, II′); 155.3 (2C, CH, II); 155.6 (2C, CH, 2; 2′). MS (FAB) *m*/*z* 773 (M−HCl).

[RuCl(tpy)(**2**)]Cl **10**: EA found C, 54.1; H, 5.8; N, 11.0. Calc. for $C_{34}H_{40}N_6OCl_2RuSi$: C, 54.5; H, 5.4; N, 11.2%. UV $\lambda_{max}(CH_2Cl_2)$/nm 241 (ε dm^3 mol^{-1} cm^{-1} 31 602), 291 (49 000), 322 (16 117), 469 (8301). IR ν, δ/cm^{-1} 2952 $\nu_{as}(CH_2, CH_3)$; 1654 ν(CN); 1616 $\nu(CC)_{tpy}$; 1598, 1559, 1458 $\nu(CC)_{bipy}$; 1381 $\delta(CH_2)$; 1251 ν(SiC); 1052br ν(SiOC); 986 δ(SiO); 772 $\delta(CH_{Ar})$. MS (FAB) *m*/*z* 749 (M + H).

*$RuCl_2$(**1**)$_2$, **11** starting with $RuCl_2(DMSO)_4$.* Organosilyldipyridine ligand **1** (200 mg, 0.49 mmol) were taken in 25 mL of dry ethanol under anaerobic conditions and 0.120 mg (0.24 mmol) of dichlorotetrakis(dimethylsulfoxide)ruthenium(II), $RuCl_2(DMSO)_4$, was added. The mixture was refluxed for 2 hours. The solvent was concentrated to half. Precipitation is obtained when dry diethylether (20 mL) was added. The brown solid is filtered and dried under vacuum giving 180 mg (0.18 mmol, 75% yield) of **11**.

$RuCl_2$(**1**)$_2$, **11**: EA found C, 41.1; H, 6.1; N, 6.3. Calc. for $C_{42}H_{66}N_6O_6Cl_2RuSi_2$: C, 41.6; H, 6.0; N, 7.4%. UV $\lambda_{max}(CH_2Cl_2)$/nm 227 (ε dm^3 mol^{-1} cm^{-1} 20 447), 292 (23 099), 380 (5663). IR ν, δ/cm^{-1} 2971, 2924 $\nu_{as}(CH_2, CH_3)$; 2882 $\nu_s(CH_3)$; 1617 ν(CN); 1551 $\nu(CC)_{bipy'}$; 1480 δ(NH); 1361 $\delta(CH_2)$; 1250 ν(SiC); 1166, 1105, 1076br ν(SiOC); 957 δ(SiO); 791 δ(CHAr). MS (IS) *m*/*z* 943 (M + H–HCl).

2.3.2 General procedures for the preparation of silica nanoparticles with incorporated ruthenium(II) complexes. Modified silica nanoparticles are denoted **SiO_2@*X*** when a ruthenium(II) complex is incorporated, ***X*** corresponds to the complex number.

Preparation of **SiO_2@3–10.** 60 mL of cyclohexane, 14.40 mL of *n*-hexanol, 14.16 mL (0.08 mmol) of Triton X-100, 0.08 mmol of complex, respectively, 78 mg (**3**), 74 mg (**4**), 54 mg(**5**), 54 mg (**6**), 54 mg (**7**), 54 mg (**8**), 62 mg (**9**), 60 mg (**10**) dissolved in 4 mL of ultra pure water, 800 μL of TEOS (dropwise) added while stirring, 480 μL of ammonia was added after 20 min and the reaction is vigorously stirred for 24 hours. Then 200 mL of acetone was added to break the microemulsion and recover the particles which were collected by centrifugation and washed several times with water and ethanol to remove any surfactant molecule and finally washed with diethylether. All washing solutions were vortexed before next centrifugation. The **SiO_2@3** to **SiO_2@10** hybrids (110–130 mg for each batch) were dried under vacuum. They are stable for more than one year at room temperature without any specific precaution. In order to check reproducibility, experiments were carried out in triplicate, incorporation ratios, τ in mmol g^{-1}, are averaged.

SiO_2@3. τ = 0.26 mmol g^{-1}. EA found: C, 11.7; H, 2.1; N, 2.5. Calc. for τ = 0.26 mmol g^{-1}: C, 10.9; H, 0.9; N, 2.5%. TGA: 0.25 mmol g^{-1}. DRIFT ν, δ/cm^{-1} 2925 $\nu_{as}(CH_2, CH_3)$; 1631 ν(CN); 1423 $\delta(CC)_{bipy}$; 1371 $\delta(CH_2)$; 1088 ν(Si–O–Si); 798 $\delta(CH_{Ar})$. ^{29}Si CP MAS NMR δ_{Si}/ppm −67 (T^3); −91 (Q^2); −100 (Q^3); −111 (Q^4). ^{13}C CP MAS NMR δ_C/ppm 9 (11), 21 (7, 10), 52 (9, 8), 124 (3′, III, 3, 5′, V, 5), 137 (IV) 151 (4′, 6, 6′, VI, 4), 157 (2′, 2, II).

SiO_2@3′. τ = 0.24 mmol g^{-1}. EA found: C, 10.4; H, 2.1; N, 2.3. Calc. for τ = 0.24 mmol g^{-1}: C 10.1; H, 0.8; N, 2.3%. TGA: 0.20 mmol g^{-1}. DRIFT ν, δ/cm^{-1} 3636 ν(OH); 1617 ν(C═N); 1560, 1541, 1466, 1448 ν(C═C); 1195, 1096br ν(Si–O–Si); 957, 806 δ(Si–O) ^{29}Si CP MAS NMR δ_{Si}/ppm −67 (T^3); −92 (Q^2); −101 (Q^3); −110 (Q^4). ^{13}C CP MAS NMR δ_C/ppm 9 (11), 21 (7, 10), 52 (9, 8), 124 (3′, III, 3, 5′, V, 5), 137 (IV) 151 (4′, 6, 6′,VI, 4), 157 (2′, 2, II).

SiO_2@4. τ = 0.22 mmol g^{-1}. EA found: C, 9.3; H, 1.2; N, 2.2. Calc. for τ = 0.22 mmol g^{-1}: C, 9.9; H, 0.9; N, 2.2%. TGA: 0.22 mmol g^{-1}. DRIFT ν, δ/cm^{-1} 2952 $\nu_{as}(CH_2, CH_3)$; 1621 ν(CN); 1464, 1445, 1422 $\nu(CC)_{bipy}$; 1086br ν(Si–O–Si); 769 $\delta(CH_{Ar})$. ^{29}Si CP MAS NMR δ_{Si}/ppm 13 (M); −100 (Q^3); −110 (Q^4). ^{13}C CP MAS NMR δ_C/ppm −1 (Si–Me); 14 (11); 21 (7, 10); 52 (9, 8); 125 (3′, III, 3); 128 (5′, V, 5′); 139 (IV); 151 (4′, 6, 6′, VI, 4); 157 (2′, 2, II).

SiO_2@4′. τ = 0.22 mmol g^{-1}. EA found: C, 10.5; H, 2.0; N, 2.2. Calc. for τ = 0.22 mmol g^{-1}: C, 9.9; H, 0.9; N, 2.2%. TGA: 0.21 mmol g^{-1}. DRIFT ν, δ/cm^{-1} 2952 $\nu_{as}(CH_2, CH_3)$; 1621 ν(CN); 1464, 1445, 1422 $\nu(CC)_{bipy}$; 1086 ν(Si–O–Si); 769 $\delta(CH_{Ar})$.

SiO_2@5. τ = 0.36 mmol g^{-1}. EA found: C, 8.2; H, 2.1; N, 1.5. Calc. for τ = 0.36 mmol g^{-1}: C, 8.1; H, 1.1; N, 1.5%. TGA: 0.20 mmol g^{-1}. DRIFT ν, δ/cm^{-1} 2915 $\nu_{as}(CH_2, CH_3)$; 1621 ν(CN); 1552 $\nu(CC)_{bipy'}$; 1481 δ(NH); 1090br $\nu(SO_S)$; ν(SiOSi); 958 δ(SiO); 464 δ(CSO).

SiO_2@6. τ = 0.40 mmol g^{-1}. EA found: C, 8.5; H, 1.8; N, 1.7. Calc. for τ = 0.40 mmol g^{-1}: C, 10.2; H, 1.5; N, 1.7%. TGA: 0.37 mmol g^{-1}. DRIFT ν, δ/cm^{-1} 1625 ν(CN); 1550 $\nu(CC)_{bipy'}$; 1480 δ(NH); 1086br ν(SiOSi; SO_S); 961 δ(SiO); 718 ν_{as}(CS); 680 ν_s(CS). ^{29}Si CP MAS NMR δ_{Si}/ppm 11 (M); −100 (Q^3); −110 (Q^4). ^{13}C CP MAS NMR δ_C/ppm −1.5 (Si–Me); 21 (7, 10); 44 (DMSO); 53 (9, 8); 124 (3′, 3, 5′, 5); 152 (4′, 6, 6′, 4); 158 (2′, 2).

SiO_2@7. τ = 0.32 mmol g^{-1}. EA found: C, 10.1; H, 1.0; N, 2.2. Calc. for τ = 0.32 mmol g^{-1}: C, 9.4; H, 0.8; N, 2.2%. TGA: 0.29 mmol g^{-1}. DRIFT ν, δ/cm^{-1} 1640 ν(CN); 1599 $\nu(CC)_{bipy'}$; 1466, 1447, 1421 $\nu(CC)_{bipy}$; 1086br ν(SiOSi); 762 $\delta(CH_{Ar})$. ^{29}Si CP MAS NMR δ_{Si}/ppm −68 (T^3); −92 (Q^2); −100 (Q^3); −109 (Q^4).

SiO_2@8. τ = 0.31 mmol g^{-1}. EA found: C, 8.5; H, 1.0; N, 2.15. Calc. for τ = 0.31 mmol g^{-1}: C, 9.9; H, 1.0; N, 2.15%. TGA: 0.29 mmol g^{-1}. DRIFT ν, δ/cm^{-1} 2922 $\nu_{as}(CH_2, CH_3)$; 1624 ν(CN); 1444, 1421 $\nu(CC)_{bipy}$; 1087br ν(SiOSi); 798

$\delta(CH_{Ar})$. ^{29}Si CP MAS NMR δ_{Si}/ppm 12 (M); −100 (Q^3); −109 (Q^4). ^{13}C CP MAS NMR δ_C/ppm −1 (Si–Me); 15 (11); 21 (7, 10); 51 (9, 8); 124.5 (3′, III, 3); 128 (5′, V, 5); 139 (IV); 151.5 (4′, 6, 6′, VI, 4); 157 (2′, 2, II).

SiO_2@9. τ = 0.20 mmol g^{-1}. EA found: C, 7.85, H, 1.6, N, 1.7. Calc. for τ = 0.20 mmol g^{-1}: C, 7.3; H, 0.6; N, 1.7%. TGA: 0.29 mmol g^{-1}. DRIFT ν, δ/cm^{-1} 1623 $\nu(CC)_{tpy}$; 1598, 1556, 1448 $\nu(CC)_{bipy}$; 1387 $\delta(CH_2)$; 1096br ν(SiOSi); 958 δ(SiO); 797 $\delta(CH_{Ar})$.

SiO_2@10. τ = 0.16 mmol g^{-1}. EA found: C: 6.7, H: 1.3, N: 1.35. Calc. for τ = 0.16 mmol g^{-1}: C, 5.8; H, 0.6; N, 1.35%. TGA: 0.16 mmol g^{-1}. DRIFT ν, δ/cm^{-1} 1640 ν(CN); 1626 $\nu(CC)_{tpy}$; 1559, 1447 $\nu(CC)_{bipy}$; 1094br ν(SiOSi); 959 δ(SiO); 801 $\delta(CH_{Ar})$. ^{29}Si CP MAS NMR δ_{Si}/ppm 12 (M); −100 (Q^3); −109 (Q^4). ^{13}C CP MAS NMR δ_C/ppm −1 (Si–Me); 15 (11); 21 (7, 10); 51.5 (9, 8); 124 (III′, III, V, 3′, 3, 5′, 5); 138 (IV, IV′); 151 (VI, 4′, 6, 6′, 4); 158 (II′, II, 2, 2′).

2.3.3 General procedures for the preparation of ruthenium(II) complexes grafted silica nanoparticles. Modified silica are denoted **SiO_2-*X*** when the ruthenium(II) complex is grafted on the silica surface, *X* corresponds to the number of the compound.

Preparation of **SiO_2-3** *to* **SiO_2-10.** 154 mg of Ludox AS-40 silica diluted with ethanol (14 mL) were reacted with 0.1 mmol of each type of complex (100 mg of **3**; 93 mg of **4**; 73 mg of **5**; 67 mg of **6**; 73 mg of **7**; 67 mg of **8**; 81 mg of **9**; 75 mg of **10**). The mixtures were stirred for 72 h at 295 K. At the end of the reaction, the sample was centrifuged at 17 000 rpm for 5 min. The clear supernatant was decanted from the solid deposit composed of the grafted particles. The obtained solid mass was washed with ethanol, dichloromethane, diethylether and then dried *in vacuo* for 2 h. Ruthenium(II) complexes grafted on silica nanoparticles (around 60 mg for each batch) **SiO_2-3** to **SiO_2-10** were acquired, except **SiO_2-5** and **SiO_2-6** nanohybrids are stable for more than one year at room temperature without any specific precaution. In order to check reproducibility, experiments were carried out in triplicate, grafting ratios, τ in mmol g^{-1}, are averaged. Solvents such as water, isopropyl-alcohol or physiological buffer were used to obtain suspension stable enough for preliminary spectroscopic studies.

SiO_2-3. τ = 0.45 mmol g^{-1}. EA found: C, 19.7; H, 1.5; N, 4.4. Calc. for τ = 0.45 mmol g^{-1}: C, 19.9; H, 1.75; N, 4.4%. TGA: 0.43 mmol g^{-1}. DRIFT ν, δ/cm^{-1} 2930 $\nu_{as}(CH_2, CH_3)$; 1619 ν(CN); 1599, 1552 $\nu(CC)_{bipy'}$; 1465, 1445, 1418 $\nu(CC)_{bipy}$; 1109br ν_{as}(Si–O–Si; BF_4); 800 δ(Si–O); 771 $\delta(CH_{Ar})$. ^{29}Si CP MAS NMR δ_{Si}/ppm −58 (T^2); −67 (T^3); −101 (Q^3); −111 (Q^4). ^{13}C CP MAS NMR δ_C/ppm, 10 (11), 21 (7, 10), 52 (9, 8), 125 (3′, III, 3, 5′, V, 5′), 138 (IV) 151 (4′, 6, 6′, VI, 4), 157 (2′, 2, II).

SiO_2-3′. τ = 0.40 mmol g^{-1}. EA found: C, 18.2; H, 1.5; N, 3.9. Calc. for τ = 0.40 mmol g^{-1}: C, 17.7; H, 1.5; N, 3.9%. TGA: 0.45 mmol g^{-1}.

SiO_2-4. τ = 0.17 mmol g^{-1}. EA found: C, 7.8; H, 1.0; N, 1.65. Calc. for τ = 0.17 mmol g^{-1}: C, 7.5; H, 0.7; N, 1.65%. TGA: 0.17 mmol g^{-1}. DRIFT ν, δ/cm^{-1} 1621 ν(CN); 1464, 1445, 1422 $\nu(CC)_{bipy}$; 1110br ν(SiOSi; BF_4); 797 $\delta(CH_{Ar})$. ^{29}Si CP MAS NMR δ_{Si}/ppm 13 (M); −101 (Q^3); −110 (Q^4). ^{13}C CP MAS NMR δ_C/ppm −1 (12); 14 (11); 20 (7, 10); 51 (C9, C8); 125 (3′, III, 3, 5′, V, 5′); 138 (IV); 151 (4′, 6, 6′, VI, 4); 157 (2′, 2, II).

SiO_2-4′. τ = 0.19 mmol g^{-1}. EA found: C, 9.1; H, 0.9; N, 1.95. Calc. for τ = 0.19 mmol g^{-1}: C, 8.8; H, 0.8; N, 1.95%. TGA: 0.20 mmol g^{-1}.

SiO_2-5. τ = 0.60 mmol g^{-1}. EA found: C, 21.24; H, 3.0; N, 2.5. Calc. for τ = 0.60 mmol g^{-1}: C, 16.4; H, 2.4; N, 2.5%. TGA: 0.62 mmol g^{-1}. DRIFT ν, δ/cm^{-1} 2915 $\nu_{as}(CH_2, CH_3)$; 1619 ν(CN); 1545 $\nu(CC)_{bipy'}$; 1112br ν(SiOSi; SO_S); 959 δ(SiO); 718 ν_{as}(CS); 682 ν_s(CS); 474 δ(CSO). ^{29}Si CP MAS NMR δ_{Si}/ppm −58 (T^2); −66 (T^3); −101 (Q^3); −110 (Q^4). ^{13}C CP MAS NMR δ_C/ppm 11 (11); 21.5 (7, 10); 46 (DMSO); 51.5 (9, 8); 125 (3′, 3, 5′, 5′); 152 (4′, 6, 6′, 4); 156 (2′, 2).

SiO_2-6. τ = 0.15 mmol g^{-1}. EA found: C, 3.5; H, 0.4; N: 0.6%. Calc. for τ = 0.15 mmol g^{-1}: C, 3.4; H, 0.5; N, 0.6%. TGA: 0.16 mmol g^{-1}. TGA: 0.17 mmol g^{-1}. DRIFT ν, δ/cm^{-1} 1623 ν(CN); 1549 $\nu(CC)_{bipy'}$; 1480 δ(NH); 1111br ν(SiOSi; SO_S); 980 δ(SiO); 718 ν_{as}(CS); 680 ν_s(CS).

SiO_2-7. τ = 0.60 mmol g^{-1}. EA found: C, 19.3; H, 2.5; N, 4.20%. Calc. for τ = 0.60 mmol g^{-1}: C, 19.4; H, 1.9; N, 4.2%. TGA: 0.62 mmol g^{-1}. DRIFT ν, δ/cm^{-1} 2920 $\nu_{as}(CH_2, CH_3)$; 1619 ν(CN); 1542 $\nu(CC)_{bipy'}$; 1477, 1444, 1421 $\nu(CC)_{bipy}$; 1112br ν(SiOSi); 798 $\delta(CH_{Ar})$. ^{29}Si CP MAS NMR δ_{Si}/ppm −58 (T^2); −67 (T^3); −101 (Q^3); −111 (Q^4). ^{13}C CP MAS NMR δ_C/ppm 11 (11); 22 (7, 10); 52 (9, 8); 126 (3′, III, 3, 5′, V, 5′) 138 (IV); 151 (4′, 6, 6′, VI, 4); 157 (2′, 2, II).

SiO_2-8. τ = 0.11 mmol g^{-1}. EA found: C, 4.05; H, 0.5; N; 0.8. Calc. for τ = 0.11 mmol g^{-1}: C, 3.7; H, 0.4; N, 0.8%. TGA: 0.20 mmol g^{-1}. DRIFT ν, δ/cm^{-1} 1623 $\nu(CC)_{tpy}$; 1112br ν(SiOSi); 962 δ(SiO).

SiO_2-9. τ = 0.29 mmol g^{-1}. EA found: C: 10.9, H: 0.7, N: 2.4. Calc. for τ = 0.29 mmol g^{-1}: C, 11.0; H, 0.9; N, 2.4%. TGA: 0.28 mmol g^{-1}. DRIFT ν, δ/cm^{-1} 3440br ν(HOSi); 2915 $\nu_{as}(CH_2, CH_3)$; 1619 $\nu(CC)_{tpy}$; 1447 $\delta(CH_3, NH)$; 1383 $\delta(CH_2)$; 1111br ν(SiOSi); 955 δ(SiO); 785 $\delta(CH_{Ar})$. ^{29}Si CP MAS NMR δ_{Si}/ppm −59 (T^2); −67 (T^3); −101 (Q^3); −110 (Q^4). ^{13}C CP MAS NMR δ_C/ppm 9.5 (11); 21 (7, 10), 50.5 (9, 8); 125 (III′, III, V, 3′, 3, 5′, 5); 138 (IV, IV′); 151 (VI, 4′, 6, 6′, 4); 158 (II′, II, 2, 2′).

SiO_2-10. τ = 0.13 mmol g^{-1}. EA found: C, 5.0; H, 0.3; N: 1.1. Calc. for τ = 0.13 mmol g^{-1}: C, 5.0; H, 0.4; N, 1.1%. TGA: 0.14 mmol g^{-1}. DRIFT ν, δ/cm^{-1} 1620 $\nu(CC)_{tpy}$; 1109br ν(SiOSi); 966 δ(SiO); 771 $\delta(CH_{Ar})$.

3. Results and discussion

3.1 Synthesis of ruthenium(II) complexes containing alkoxysilyldipyridine ligands

Starting with ruthenium(II) complexes known for their stability and reactivity, such as $RuCl_2(bpy)_2$, $RuCl_2(DMSO)_4$, $RuCl_3(tpy)$, five types of complexes containing at least one dipyridine ligand involving an organosilane function as

triethoxy- or ethoxydimethyl-silane have been synthesized (Scheme 3). All the reactions were carried out refluxing in acetone or ethanol for a few hours under an inert atmosphere according to the hydrolysis of the alkoxysilane group. Brown to red powders were isolated in good yield (53–98%) for all complexes with different silane groups.

We have synthesized the complexes from $RuCl_2(bpy)_2$ using procedures similar to those for $[Ru(bpy)_3]^{2+}$ according to Sullivan's procedure,[27] but using a silver salt. Chloride and tetrafluoroborate salts have been synthesized to study the influence of the counteranion on the incorporation reaction. The reaction may be separated into two substitution steps. First, the chloro ligands are extracted by the silver salt and replaced by two acetone molecules, second is the substitution of the labile acetone ligands by the dipyridine ligand. The first step is monitored by UV-visible spectrometry indicating that four hours refluxing in acetone are needed to extract the chloro ligands leading to $[Ru(bpy)_2(acetone)_2]^{2+}$. This complex is separated by filtration and used without further purification in a reaction with 1.5 equivalents of organosilane, leading to $[Ru(bpy)_2(\mathbf{1})](BF_4)_2$, **3** (98%) or $[Ru(bpy)_2(\mathbf{2})](BF_4)_2$, **4** (71%) after 3 h in refluxing solvent.

In order to modify the heterocyclic ligand on the ruthenium, terpyridine was chosen for its electronic properties. As tridentate ligand it leads to the monocationic ruthenium(II) complexes [RuCl(tpy)(**1**)]Cl, **9**, and [RuCl(tpy)(**2**)]Cl, **10**, starting with $RuCl_3(tpy)$. The chloro ligand substitution on the $RuCl_3(tpy)$ precursor is carried out in refluxing ethanol, a solvent leading to the reduction to ruthenium(II). The synthesis is adapted from the procedure proposed by L. Dudd *et al.*[32] using triethylamine to extract chloride with an excess of ligand to isolate the expected complexes **9** and **10** after four hours refluxing in 65% and 59% yields respectively.

Two types of complexes were synthesized using $RuCl_2(DMSO)_4$ as the inorganic precursor, leading to $RuCl_2(DMSO)_2(\mathbf{1})$, **5**, and $RuCl_2(DMSO)_2(\mathbf{2})$, **6**. The reaction was carried out under

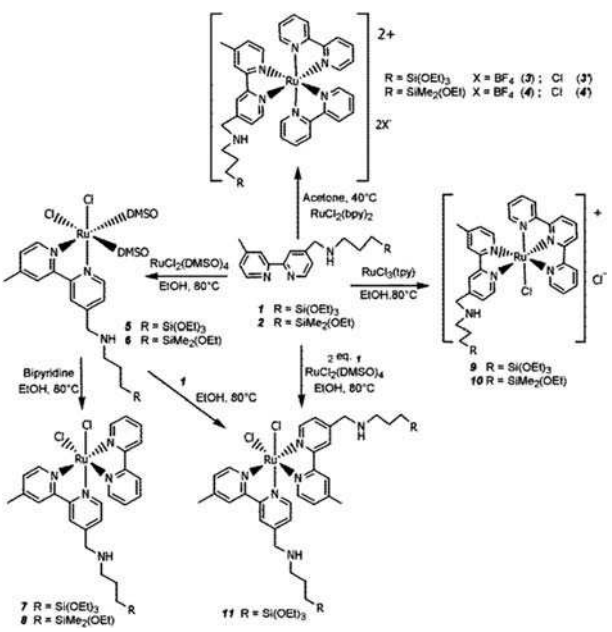

Scheme 3 Synthesis of silylated ruthenium(II) complexes (**3–11**).

stoichiometric conditions and after two hours refluxing in ethanol, powders were isolated by precipitation with diethylether giving rise to **5** and **6** in 53% and 60% yields, respectively. These complexes have two labile DMSO ligands of interest for further reactions, leading to the possibility of introducing organic molecules into the coordination sphere. These molecules can act as coupling, recognizing or addressing agents binding biological substrates to the luminescent particles. In our case, we illustrate this reactivity by the reaction with 2,2′-dipyridine. Refluxing **5** and **6**, two hours with one equivalent of 2,2′-dipyridine we obtained $RuCl_2(bpy)(\mathbf{1})$, **7**, and $RuCl_2(bpy)(\mathbf{2})$, **8**, with 62% and 30% yields, respectively. Complex **8** is isolated with a lower yield because of its higher solubility. A similar complex **11**, $RuCl_2(\mathbf{1})_2$, containing two silylated dipyridine has been obtained using ligand **1** instead of the additional dipyridine to substitute the two last DMSO ligands in **5**. Direct reaction of two equivalents of ligand **1** with $RuCl_2(DMSO)_4$ in refluxing ethanol for two hours gives the same complex **11** which is obtained by this protocol in higher yield. Because of its very low solubility in water, this complex has not been used for further nanomaterial synthesis in this work.

The stoichiometry for all complexes is in agreement with elemental analysis and mass spectrometry. The isotopic pattern of the molecular peak in the mass spectra is in agreement with the formula. The dipyridine ligands lead to intense MLCT transitions in the UV-visible range assigned as summarized in Table 1. UV spectra of organosilanes have two strong absorption bands (ε = 10 000–19 000 $dm^3\ mol^{-1}\ cm^{-1}$) corresponding to π–π* transitions. All complexes show broad and intense MLCT absorption bands, and the complexation effect is illustrated by the increase of intensity and by a small shift observed for all transitions as indicated in Table 1. Well defined luminescence spectra, recorded on powder samples for all complexes, are discussed in the following section.

The coordination of the organosilane ligand is confirmed by IR analysis through the ring stretching vibrations of dipyridine, the CH_3, CH_2 and NH stretching and bending vibrations of the propyl chain and secondary amino function, and the Si–O stretching and bending of the alkoxysilyl group. IR spectra of complexes **4**, **6**, **8** and **10** containing the monoethoxysilylated dipyridyl ligand differ from those of complexes **3**, **5**, **7** and **9**, containing triethoxysilylated dipyridyl ligands, by the more intense ν_{Si-C} stretching vibration in the 1250–1254 cm^{-1} range, in agreement with the presence of two methyl groups of the silane function in ligand **2**. In addition to the usual vibrations, some bands are specific and due to the counteranion with ν_{B-F} at 1055 cm^{-1}

Table 1 UV absorption maxima of organosilanes **1** and **2** and ruthenium complexes **3–10** (λ in nm, ε in $dm^3\ mol^{-1}\ cm^{-1}$)

Compound	π–π* L	d–π* (MLCT)	π–π* L	d–π*(MLCT)
bpy	241 (9935)		284 (13 835)	
1	243 (10 349)		284 (11 788)	
2	240 (16 829)		283 (19 168)	
3		254 (45 996)	290 (96 920)	458 (10 670)
4		246 (74 856)	286 (78 617)	453 (9648)
5		226 (21 465)	290 (24 601)	435 (2057)
6		227 (20 447)	292 (23 099)	380 (5663)
7		228 (8189)	290 (8637)	466 (1213)
8	240 (21 859)	288 (43 503)	424 (3067)	455 (4024)
9	239 (24 000)	284 (30 682)	318 (5955)	
10	241 (31 602)	291 (49 000)	322 (16 117)	469 (8301)

for **3** and **4**; the S-coordinated DMSO ligand with S–O streching vibrations ν_{S-O} at 1190 and 1179 cm^{-1} for **5** and **6**, respectively, or the terpyridine ligand characterized by a narrow but intense carbon–carbon stretching vibration $\nu_{c=c}$ at 1616 cm^{-1} in **9** and **10** complexes.

Finally, the characterization by $^{13}C\{^{1}H\}$NMR allows us to assign all magnetically inequivalent carbon atoms in each complex. Signals at 54 and 18 ppm observed for all compounds indicate the presence of at least one ethoxysilane function. Compounds **4**, **6**, **8** and **10** exhibit a low field resonance at 0 ppm assigned to the methyl groups of the silane **2**. Signals at approximately 125, 138, 151 and 157 ppm for the dipyridyl moiety of the two types of dipyridine derivatives, and those in the range 9–12.5; 21–24 and 50–52 ppm indicate the presence of the propyl chain. The peak at 20 ppm, also assigned to the methyl substituent of the organosilyldipyridine ligand, is identified in each spectrum. The spectra of compounds **5** and **6** differ from the others by the presence of a signal at 43–45 ppm assigned to the methyl groups of DMSO ligands whereas signal at 138 ppm is specific of the dipyridine molecule observed in compounds **3**, **4**, **7** and **8**.

We have two different sets of luminescent ruthenium(II) precursors: molecular complexes **5**, **6**, **7** and **8** and cationic complexes **3**, **4**, **9** and **10**. With the aim to study the effect of the counterion of the dye molecules in the incorporation reaction, we have also synthesized the chloride derivative of **3** noted **3′**. All data are in agreement with those of the tetrafluoroboride derivative with the exception of the water solubility, which is thoroughly increased.

3.2 Metallated nanohybrids

3.2.1 Silica nanoparticles incorporating silylated Ru(II) complexes, SiO_2@X. Dye doped silica nanoparticles are obtained using ammonia-catalysed hydrolysis of tetraethoxysilane (TEOS) in a quaternary water-in-oil microemulsion of Triton X100–cyclohexane–hexanol–water, where hexanol is a cosurfactant, according to the procedure described by Tan *et al.*[33] This method has advantages in that particle size, monodispersity and shape can be simply controlled by varying microemulsion parameters such as the nature of the surfactant, the concentrations of TEOS and ammonia, the water to surfactant molar ratio, and the cosurfactant to surfactant molar ratio. Thus it is possible to obtain particle sizes smaller than 100 nm with a good monodispersity. As reported by these authors, the particle size decreases as the concentration of the cosurfactant increases and the monodispersity of the particles increases. The syntheses were adapted to the previously synthesized complexes and we target particle sizes in the range 40–70 nm. In this way, the water to surfactant molar ratio was fixed at 9.6, the cosurfactant to surfactant molar ratio was fixed at 5 with an *h* hydrolysis factor corresponding to a water to TEOS molar ratio equals 50 with an ammonia concentration of 0.2 wt%.

Under these conditions, new silylated-dipyridine ruthenium(II) complexes are incorporated in the same amount than that observed for the unsilylated $[Ru(bpy)_3]Cl_2$ complex[33] giving rise to luminescent nanoparticles. In our experimental conditions incorporation ratios are in the range 0.16–0.40 mmol of complex per gram of silica (see details in Table 2).

Surprisingly, molecular complexes (**5–8**) lead to higher incorporation ratios (0.31–0.40 mmol g^{-1}) than cationic complexes (0.16–0.26 mmol g^{-1}) for both the triethoxy-(**1**) or the monoethoxy-(**2**) silanes. Because of the presence of three hydrolysable functions, complexes containing ligand **1** was preferred for incorporation reaction. Another important result is the morphology of the obtained particles indicating that generally in our experimental conditions well-defined spherical particles with a good monodispersity are obtained. Different average particle sizes are obtained in the range 41–80 nm according to the nature of the incorporated complex. In our experimental conditions, the average size of the $[Ru(bpy)_3]^{2+}$ doped particles is in the range of 47–50 nm, as shown in Fig. 1a, in agreement with the value announced by Tan *et al.*[33] In contrast the size of the particles doped with $RuCl_2(DMSO)_2$(**1**), **SiO_2@5** (Fig. 1c), increases to 70 nm whereas the size of the particles incorporating $RuCl_2$(bpy)(**1**), **SiO_2@7**, remains around 50 nm (Fig. 1b). The change in the molecular structure of the complexes involves the modification of the particle size. SEM analysis indicates also that tetrafluoroborate salt (*i.e.* complexes **3**, **4**) is not convenient for the incorporation reaction whereas the corresponding chloride salt leads to well-defined spherical nanoparticles as illustrated in SEM micrographs for **SiO_2@3** (Fig. 1d) and **SiO_2@3′** (Fig. 1e).

The size of individual and spherical nanoparticles were obtained, it slightly decreases to 41 nm for the **SiO_2@3′**

Table 2 Incorporation or grafting ratios and size of metallated nanohybrids

Complex number	Compounds	Incorporation ratio in mmol g^{-1} of silica **SiO_2@*X***	Particle size/nm	Grafting ratio in mmol g^{-1} of silica **SiO_2-*X***	Particle size[a]/nm
	$[Ru(bpy)_3]^{2+}$	0.30	50 ± 2	—	
	Ligand **1**			1.24	
	Ligand **2**			0.28	
3	$[Ru(bpy)_2(\mathbf{1})]^{2+}(BF_4)_2$	0.26		0.45	27 ± 2
3′	$[Ru(bpy)_2(\mathbf{1})]^{2+}Cl_2$	0.24	41 ± 2	0.40	27 ± 2
4	$[Ru(bpy)_2(\mathbf{2})]^{2+}(BF_4)_2$	0.22		0.17	27 ± 2
4′	$[Ru(bpy)_2(\mathbf{2})]^{2+}Cl_2$	0.22		0.19	27 ± 2
5	$RuCl_2(DMSO)_2(\mathbf{1})$	0.36	70 ± 3	0.60	27 ± 2
6	$RuCl_2(DMSO)_2(\mathbf{2})$	0.40		0.15	27 ± 2
7	$RuCl_2$(bpy)(**1**)	0.32	48 ± 2	0.60	27 ± 2
8	$RuCl_2$(bpy)(**2**)	0.31		0.11	25 ± 2
9	[RuCl(tpy)(**1**)]Cl	0.20	50–80	0.29	27 ± 2
10	[RuCl(tpy)(**2**)]Cl	0.16		0.13	27 ± 3

[a] Size of Ludox starting particles is 23 ± 2 nm.

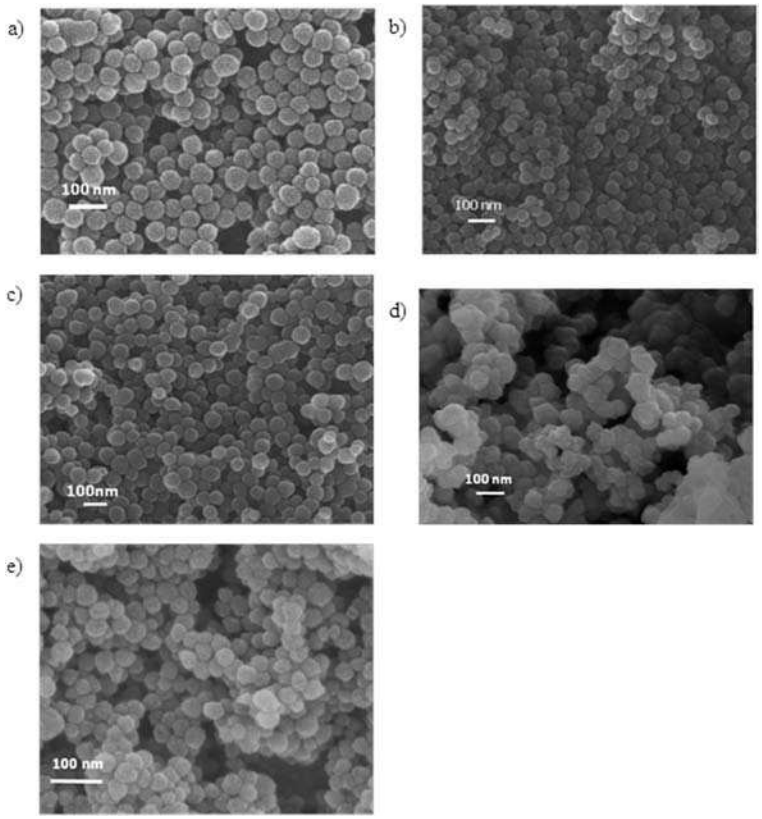

Fig. 1 FE-SEM micrographs of complex incorporated nanoparticles (a) **SiO_2@[Ru(bpy)$_3$]**; (b) **SiO_2@7**; (c) **SiO_2@5**; (d) **SiO_2@3**; (e) **SiO_2@3′**.

incorporating $[Ru(bpy)_2(\mathbf{1})]^{2+}$ complexes, closely related to $[Ru(bpy)_3]^{2+}$. Histograms of particle size of nanohybrids are presented in Fig. 2 together with TEM micrographs for **SiO_2@3′** (Fig. 2a, 41 ± 3 nm) and **SiO_2@7** (Fig. 2b, 48 ± 2 nm). In all cases, the presence of alkoxysilyl group of the dipyridine ligands improves the immobilisation of the complex in the bulk of silica preventing the release of the dye as observed when $[Ru(bipy)_3]Cl_2$ is used. Using silylated complexes, the experimental protocol is easier, limiting the number of washings, giving more stable dye doped nanoparticles. In the incorporation experiment, in opposition to the grafting reaction which will be detailed below, complexes containing ligand **1** are preferred to those with monoethoxysilane ligand **2** according to the number of siloxane bond expected even if the incorporation ratio is retained.

Table 3 reports ^{29}Si CP MAS NMR data for each type of metallated silica nanoparticles with assignments using terminology suitable for silica based hybrids.[34,35] Incorporation of the ruthenium complexes *via* siloxane covalent bonds is confirmed by the ^{29}Si CP MAS NMR spectra of **SiO_2@3′** and **SiO_2@7** which present only T^3 silicon atoms at lower field (∼−68 ppm) indicating that all the alkoxysilane functions are condensed on the bulk of the particles. As expected only one signal, corresponding to the siloxane bond to the matrix, appeared at lower field (∼12 ppm) for the M^1 silicon atom of ligand **2** for **SiO_2@4**,**6**,**8**,**10** nanohybrids. High field signals (−91, −100 and −110 ppm) are assigned to the Q^{2-4} silicon atom types of the silica shell indicating the presence of free silanol sites.

3.2.2 Silylated Ru(II) complexes grafted on silica nanoparticles, SiO_2-*X*. All silylated complexes were used in grafting reactions in a 1 : 10 (v/v) water and ethanol mixture at 295 K during 72 h. In this reaction, the amount of introduced complex Ω in mmol per gram of silica is higher than for the incorporation reaction and fixed to 1.6 according to our previous results describing the functionalization of silica nanoparticles with organosilanes **1** and **2**. The silanization reagent is used in large excess toward the support in order to saturate the silanol sites of the silica matrix, a well-established procedure for grafting reaction. In our case, a compromise was made between the excess needed and the quantities of synthesized complexes available. Grafting ratios are reported in Table 2 and NMR data are summarized in Table 3. Because the grafting reaction is heterogeneous, it leads to a wide range of grafting ratio values (0.11 to 0.60 mmol g^{-1}), depending on the type of complexes compared to those obtained with the incorporation method (0.16 to 0.40 mmol g^{-1}), where the reaction between molecular silica precursors, TEOS, and the silylated complexes is favoured. As expected for triethoxysilane derivatives, grafting ratios are higher than those obtained with complexes containing ligand **2** since grafting ratios decrease from 0.29–0.60 to 0.11–0.19 mmol of complex per gram of silica. This result is in agreement with the difference of grafting ratios previously reported for the grafting of the free ligands[16] (1.24 for **1** and 0.28 for **2**). Moreover, in all cases grafting ratios of complexes are lower than those observed for the free ligands because of the lower accessibility of the alkoxysilane function to condense with silanol sites due to the hindrance of the complexes.

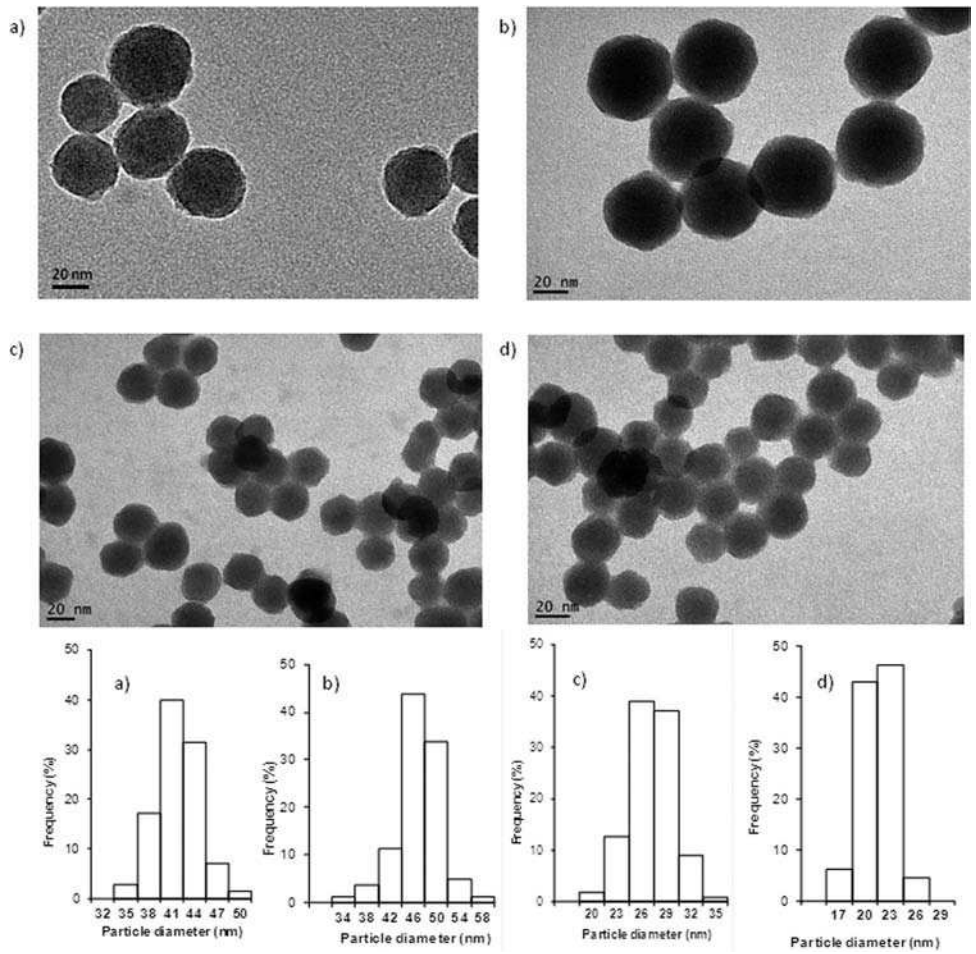

Fig. 2 TEM micrographs of both types of metallated silica nanoparticles and histograms below: (a) **SiO_2@3′**; (b) **SiO_2@7** (c) **SiO_2-7**; (d) Ludox silica.

Table 3 ^{29}Si NMR data for metal grafted or incorporated nanohybrids

	Compound	Chemical shift δ/ppm
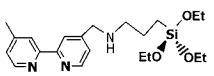	**1**	−45.3[a]
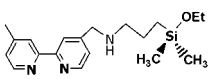	**2**	7.6[a]
$[Ru(bpy)_2$(**1**)$]Cl_2$	**SiO_2@3′**	−67; −91; −100; −111
$[Ru(bpy)_2$(**2**)$]Cl_2$	**SiO_2@4′**	13; −100; −110
$RuCl_2(DMSO)_2$(**1**)	**SiO_2@5**	
$RuCl_2(DMSO)_2$(**2**)	**SiO_2@6**	11; −100; −110
$RuCl_2$(bpy)(**1**)	**SiO_2@7**	−68; −92; −100; −109
$RuCl_2$(bpy)(**2**)	**SiO_2@8**	12; −100; −109
[RuCl(tpy)(**1**)]Cl	**SiO_2@9**	
[RuCl(tpy)(**2**)]Cl	**SiO_2@10**	12; −100; −109
$[Ru(bpy)_2$(**1**)$](BF_4)_2$	**SiO_2-3**	−58; −67; −101; −111
$[Ru(bpy)_2$(**2**)$](BF_4)_2$	**SiO_2-4**	13; −101; −110
$RuCl_2(DMSO)_2$(**1**)	**SiO_2-5**	−58; −66; −101; −110
$RuCl_2(DMSO)_2$(**2**)	**SiO_2-6**	
$RuCl_2$(bpy)(**1**)	**SiO_2-7**	−58; −67; −101; −111
$RuCl_2$(bpy)(**2**)	**SiO_2-8**	
[RuCl(tpy)(**1**)]Cl	**SiO_2-9**	−59; −67; −101; −110
[RuCl(tpy)(**2**)]Cl	**SiO_2-10**	

[a] $CDCl_3$.

This effect is emphasized for complexes containing ligand **2** which exhibits only one hydrolysable function. Here on top of minimizing the amount of water to Ludox sol, the oligomerisation of the complex is limited by the hindrance of the complex on the silica surface leading to a monolayer of ruthenium(II) complexes grafted on the surface of silica nanoparticles. Low grafting ratios of the complexes containing ligand **1** result also in a near monolayered or very small oligomers grafted nanoparticles.

Nevertheless, for complexes containing ligand **1**, grafting ratios, τ, are higher than those obtained by incorporation and these values can be tuned according to two parameters. First is the steric hindrance of the complex. We can see in Table 2 that grafting ratio increases when hindrance of the complex, related to the presence of dipyridine/terpyridine ligands in the coordination sphere of the ruthenium, decreases as illustrated by the values of 0.60 mmol g^{-1} obtained for **SiO_2-5** and **SiO_2-7** and the lower values (0.45 and 0.29 mmol g^{-1}) obtained, respectively, for **SiO_2-3** and **SiO_2-9**. The second parameter is the introduced amount (Ω) during the hybrid synthesis. Grafting ratio, τ, decreases parallel to Ω since a grafting ratio of 0.30 mmol g^{-1} is obtained when only 1.0 mmol of **3** is introduced (not in Table 2). It has to be noticed that the influence of the counter anion, tetrafluoroborate or chloride, observed in the incorporation protocol for complexes **3** and **3′**, is cancelled for the grafting reaction because no destabilisation of the media occurred by opposition of the destabilisation observed in the reverse microemulsion.

Another difference between nanohybrids obtained by grafting or incorporation is that for all grafted hybrids the particle size slightly increases from 23 nm for the starting particles to 27 nm and the monodispersity is retained indicating that morphology (form, size and dispersity) of the hybrid is really dependent on the properties of the starting particles. A TEM micrograph of metal grafted nanohybrids is illustrated in the case of **SiO_2-7** (Fig. 2c) and compared to the Ludox silica as starting particles (Fig. 2d). This result is interesting and highlights the possibility to design nano-sized metallated luminescent hybrids **SiO_2@*X*** or **SiO_2-*X*** according to the chemical nature of the metal complex, its introduced amount and finally the morphology of the silica matrix.

Covalent grafting is confirmed by ^{29}Si CP MAS NMR analysis with the presence of −58 and −67 ppm signals assigned to T^2 and T^3 silicon atoms, respectively, indicating that in this case condensation of the trialkoxysilane group is not always completed. Of course the bulk of silica is characterized by the Q^3 and Q^4 silicon atoms at −100 and −110 ppm, respectively, as already observed for previous dye doped particles **SiO_2@*X*** (*X*: **3–10**). ^{29}Si solid state NMR highlights different surface properties of both types of nanohybrids, this can be observed in Fig. 3 where CP MAS (left) and MAS (right) ^{29}Si NMR spectra are compared for **SiO_2-3**(top) and **SiO_2@3′**(bottom). We can see with evidence that nanohybrids incorporating the dye exhibit an intense signal corresponding to silanol sites (Q^3) whereas these sites have partly reacted during grafting reaction of the silylated complex. Because spectra were recorded under quantitative conditions, deconvolution of the curves were undertaken using DMfit program[31] indicating a Q^3/Q^4 proportion of 15/85 for grafted particles whereas this proportion reaches 45/55 for complex incorporated nanohybrids. As expected **SiO_2@*X*** hybrids present higher amount of silanol sites on the surface for further reactivity as described in Scheme 2a to obtain bifunctionalized silica nanoparticles.

Details of characteristic data obtained by DRIFT and ^{13}C CP MAS NMR spectroscopies reported in the experimental section show that the chemical integrity of the complexes is retained on the silica surface. As an example, Fig. 4 shows NMR spectra of complex **3**, $[Ru(bpy)_2(\mathbf{1})]^{2+}$, for the free complex in solution (a), solid state NMR of the corresponding nanohybrids **SiO_2@3** (b) and **SiO_2-3** (c). ^{13}C NMR spectra

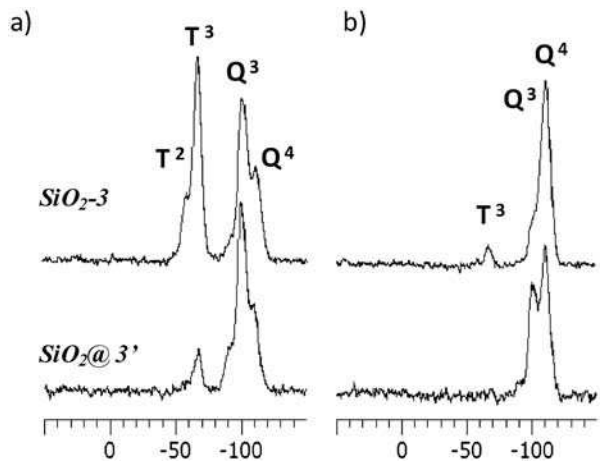

Fig. 3 ^{29}Si solid state NMR spectra of **SiO_2-3** (top) and **SiO_2@3′** (bottom) in CP MAS experiment (a) and MAS experiment (b).

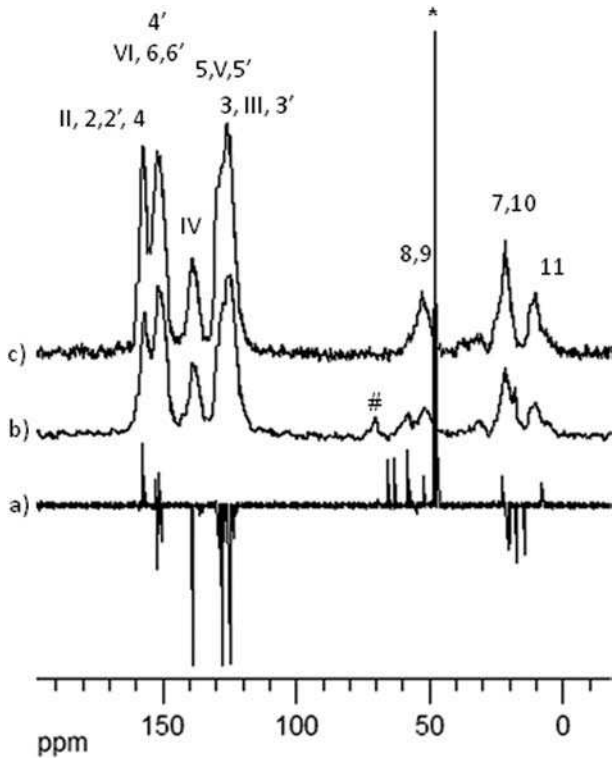

Fig. 4 $^{13}C\{^1H\}$ NMR spectra of free complex **3** in CD_3OD (a); ^{13}C CP MAS NMR of **SiO_2@3′** (b); **SiO_2-3** (c).

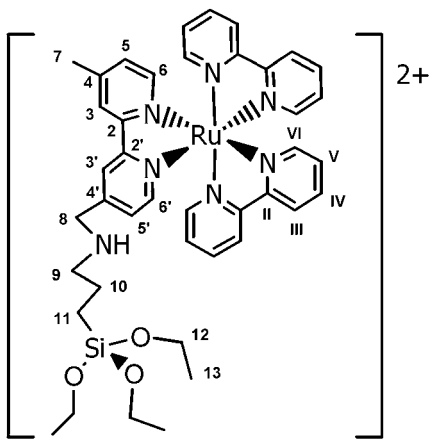

Scheme 4 Carbon atom numbering for cationic complexes **3** and **3′**.

exhibit the chemical shifts expected for each type of carbon atoms of the propyl chain, the methyl substituent of ligand **1**, each carbon atom of the unsubstituted and substituted bipyridine ligands, despite the broadening of the spectra due to the anisotropy of the solid state. Assignments in Fig. 4 are given according to the carbon atom numbering (Scheme 4).

3.3 Luminescence properties of nanomaterials

Both types of metallated nanohybrids, containing dipyridine ruthenium(II) complexes as luminophore, exhibit spectral features similar to those of the well known dye doped silica nanoparticles obtained by encapsulation of $[Ru(bipy)_3]Cl_2$ with an intense MLCT band with maxima in the 620–810 nm

Table 4 Wavelengths of luminescence band maxima for free complexes and SiO_2-*X* and SiO_2@*X* metallated nanohybrids, solid state, $\lambda_{exc.}$ = 488 nm

	Complex number	Free complex	SiO_2-*X*	SiO_2@*X*
$[Ru(bpy)_3]Cl_2$		620	—	660
$[Ru(bpy)_2$(**1**)$]Cl_2$	**3′**	716	700	680
$[Ru(bpy)_2$(**2**)$]Cl_2$	**4′**	700	720	675
$RuCl_2(DMSO)_2$(**1**)	**5**	780	790	700
$RuCl_2(DMSO)_2$(**2**)	**6**	810	695	700
$RuCl_2$(bpy)(**1**)	**7**	790	790	667
$RuCl_2$(bpy)(**2**)	**8**	790	690	750
[RuCl(tpy)(**1**)]Cl	**9**	750	750	750
[RuCl(tpy)(**2**)]Cl	**10**	760	740	755

range as reported in Table 4. The luminescence spectra show that luminescence properties of the ruthenium(II) complexes are retained.

Luminescence maxima and bandwidths are similar to those observed for $[Ru(bpy)_3]^{2+}$ as illustrated in Fig. 5 (spectra in physiological buffer) and Fig. 6 and 7 (solid state spectra) for dye incorporated or grafted nanohybrids in agreement with previously reported spectra for nanohybrids[2] or free complexes.[36]

An intriguing feature is the intensity of the emission for dye grafted or incorporated nanohybrids since, despite the diluted conditions of approximately 1% doped in both nanohybrids, comparable luminescence intensities are systematically observed, pointing towards a promising approach to new efficient luminescent hybrid nanomaterials.

The shifts of maxima and changes in bandwidths observed in the series of ruthenium(II) complexes are most likely due to the different environment of the dye in each type of hybrid: the luminophore can be located on the surface or in the bulk of the silica matrix. With the exception of the terpyridine complexes, the emission of surface grafted nanoparticles is red shifted compared to the nanoparticles with bulk incorporated complexes, indicating transitions at lower energy most likely due to a stronger stabilization of the acceptor excited state in SiO_2@*X* than in SiO_2-*X* or in the pure complexes.

Fig. 5–7 show that broad bands are observed for incorporated complexes, a likely consequence of different environments within the doped nanoparticles. Grafted nanoparticles show bandwidths almost similar to those of the pure complex, indicative of a more homogeneous ensemble of luminescent complexes.

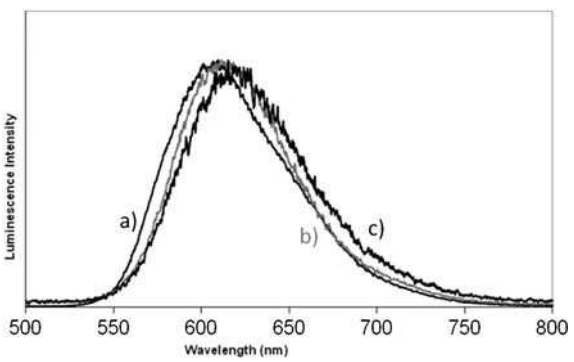

Fig. 5 Luminescence emission spectra of SiO_2@[$Ru(bpy)_3$] (a), SiO_2@**4** (b grey) and SiO_2@**7** (c), $\lambda_{exc.}$ = 290 nm, physiological buffer.

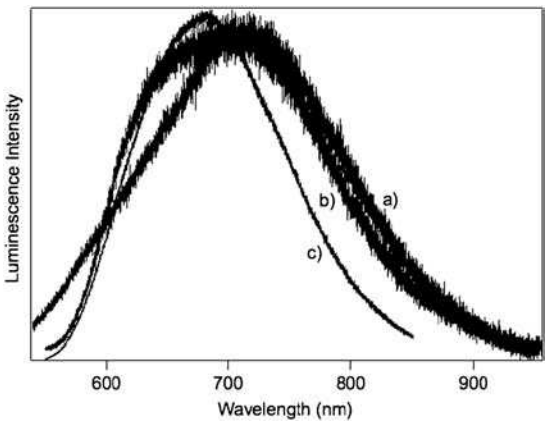

Fig. 6 Solid-state luminescence spectra of **3** (a), SiO_2@**3′** (b) and SiO_2-**3** (c), $\lambda_{exc.}$ = 488 nm.

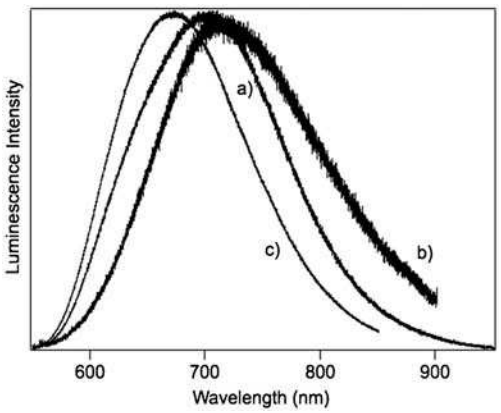

Fig. 7 Solid-state luminescence spectra of **4** (a), SiO_2@**4′** (b) and SiO_2-**4** (c), $\lambda_{exc.}$ = 488 nm.

The band maxima for incorporated nanoparticles are shifted to lower energy, those of grafted nanoparticles in Fig. 6 and 7 to higher energy than the pure compound. This trend is interesting, as it might lead to less efficient quenching for the higher-energy luminescence and the luminescence spectra show clear differences between encapsulated and grafted nanoparticles. Moreover, for grafted nanohybrids, the luminescence intensity appears to be dependent on the grafting ratio, an aspect that needs to be further explored.

4. Conclusion

We have synthesized new MLCT ruthenium(II) complexes containing silylated-dipyridine ligands. The two novel luminescent materials (bulk or surface grafted) are different in size and in the localisation of the dye. We have shown that using complexes containing one alkoxysilyl group in a grafting reaction leads to monolayer-grafted silica nanoparticles with both mono- and trialkoxysilane derivatives. Nanosized and monodispersed particles are characterized; size can be tuned through the incorporation of different types of ruthenium(II) complexes. Both grafting and incorporation ratios can be controlled. Solid state NMR has proven to be a powerful tool for the characterization of the chemically modified nanohybrids indicating a homogeneous distribution of the complex,

in the core or on the surface of the nanoparticles. The chemical integrity of the complexes is retained during both grafting and incorporation procedures. The two approaches described here are complementary, allowing us to modulate the size of the nanohybrid through the choice of the incorporated complex, the morphology of the silica matrix and the amount of luminophore. Bulk bonded ruthenium(II) silica based hybrids are now available as luminescent platforms for further surface functionalization. Coordination chemistry on metal complexes grafted on the silica surface is currently being developed in order to develop various sophisticated hybrids.

Acknowledgements

This work was supported by the CNRS and the Ministère de la Recherche en France. S. C.; L. M. and S. R. K. thank MESR and Université Toulouse III-Paul Sabatier, respectively, for a grant. The authors thank F.-G. Rollet for assistance with luminescence measurements and D. Massiot for using Dmfit program for fitting solid state NMR spectra. Support of this collaboration through a Journals grant for international authors (Royal Society of Chemistry) to C. R. is gratefully acknowledged.

References

1 N. Zhu, H. Cai, P. He and Y. Fang, *Anal. Chim. Acta*, 2003, **481**, 181.
2 L. Qian and X.-R. Yang, *Adv. Funct. Mater.*, 2007, **17**, 1353.
3 X. Liu, Z. Ma, J. Xing and H. Liu, *J. Magn. Magn. Mater.*, 2004, **270**, 1.
4 J. Lee, Y. Lee, J. K. Youn, H. B. Na, T. Yu, H. Kim, S.-M. Lee, Y.-M. Koo, J. H. Kwak, H. G. Park, H. N. Chang, M. Hwang, J.-G. Park, J. Kim and T. Hyeon, *Small*, 2008, **4**, 143.
5 X. Zhao, R. â. P. Bagwe and W. Tan, *Adv. Mater.*, 2004, **16**, 173.
6 L. M. Rossi, L. Shi, F. H. Quina and Z. Rosenzweig, *Langmuir*, 2005, **21**, 4277.
7 S. Santra, P. Zhang, K. Wang, R. Tapec and W. Tan, *Anal. Chem.*, 2001, **73**, 4988.
8 L. Wang, K. Wang, S. Santra, X. Zhao, L. R. Hilliard, J. E. Smith, Y. Wu and W. Tan, *Anal. Chem.*, 2006, **78**, 646.
9 L. Wang, W. Zhao and W. Tan, *Nano Res.*, 2008, **1**, 99.
10 D. Knopp, D. Tang and R. Niessner, *Anal. Chim. Acta*, 2009, **647**, 14.
11 W. Lian, S. A. Litherland, H. Badrane, W. Tan, D. Wu, H. V. Baker, P. A. Gulig, D. V. Lim and S. Jin, *Anal. Biochem.*, 2004, **334**, 135.
12 J. E. Smith, L. Wang and W. Tan, *TrAC, Trends Anal. Chem.*, 2006, **25**, 848.
13 V. Marin, E. Holder and U. S. Schubert, *J. Polym. Sci., Part A: Polym. Chem.*, 2004, **42**, 374.
14 P. G. Pickup and K. R. Seddon, *J. Chem. Soc., Dalton Trans.*, 1991, 489.
15 S. Benyahya, F. Monnier, M. Taillefer, M. Wong Chi Man, C. Bied and F. Ouazzani, *Adv. Synth. Catal.*, 2008, **350**, 2205.
16 S. Cousinié, M. Gressier, P. Alphonse and M.-J. l. Menu, *Chem. Mater.*, 2007, **19**, 6492.
17 P. Ghosh and T. G. Spiro, *J. Am. Chem. Soc.*, 1980, **102**, 5543.
18 E. Johansson and J. I. Zink, *J. Am. Chem. Soc.*, 2007, **129**, 14437.
19 S. Cousinie, M. Gressier, C. Reber, J. Dexpert-Ghys and M.-J. Menu, *Langmuir*, 2008, **24**, 6208.
20 S. Paulson, K. Morris and B. P. Sullivan, *Chem. Commun.*, 1992, 1615.
21 Y. Duan, G.-A. Wen, W. Wei, J.-C. Feng, G.-Q. Xu and W. Huang, *Thin Solid Films*, 2008, **517**, 469.
22 S. Zanarini, E. Rampazzo, L. D. Ciana, M. Marcaccio, E. Marzocchi, M. Montalti, F. Paolucci and L. Prodi, *J. Am. Chem. Soc.*, 2009, **131**, 2260–2267.
23 G. Kickelbick, in *Hybrid Materials. Synthesis, Characterization and Applications*, ed. G. Kickelbick, Wiley-VCH, 2007, ch. 1, pp. 3–5.
24 C. M. Carbonaro, A. Anedda, S. Grandi and A. Magistris, *J. Phys. Chem. B*, 2006, **110**, 12932.
25 M.-J. Li, Z. Chen, V. W.-W. Yam and Y. Zu, *ACS Nano*, 2008, **2**, 905.
26 Silylated dipyridine ligand characterization: **1** UV $\lambda_{max}(CH_2Cl_2)$/nm 243 (ε dm^3 mol^{-1} cm^{-1} 10 349), 284 (11 788). IR ν, δ/cm^{-1} 3308 ν(NH); 2928 $\nu_{as}(CH_3, CH_2)$; 2884 $\nu_s(CH_3, CH_2)$; 1595, 1555, 1456 $\nu(CC)_{bipy}$; 1376 $\delta(CH_2)$; 1269 ν(SiC); 1076 ν(SiOC); 958 δ(Si–O); 736 $\delta(CH_2,CH_3)$. ^{1}H NMR δ_H(300.13 MHz; $CDCl_3$; ppm) 0.65 (2H, m, CH_2, 11-H); 1.21 (9H, t, J_{AB} = 7, CH_3, H-13); 1.64 (2H, m, CH_2, H-10); 2.41 (3H, s, CH_3, 7-H); 2.65 (2H, m, CH_2, 9-H); 3.79 (6H, q, J_{AB} = 7, CH_2, 12-H); 3.89 (2H, s, CH_2, 8-H); 7.13 (1H, d, J_{AB} = 6, CH, 5′-H); 7.26 (1H, d, J_{AB} = 6, CH, 5-H); 8.22 (1H, s, CH, 3′-H); 8.31 (1H, s, CH, 3-H); 8.53 (1H, d, J_{AB} = 6, CH, 6′-H); 8.61 (1H, d, J_{AB} = 6, CH, 6-H). $^{13}C\{^1H\}$ NMR δ_C(75.5; $CDCl_3$; ppm) 7.9 (1C, CH_2, 11); 18.3 (3C, CH_3, 13); 21.2 (1C, CH_3, 7); 23.4 (1C, CH_2, 10); 52.3 (1C, CH_2, 9); 53.4 (1C, CH_2, 8); 58.2 (3C, CH_2, 12); 120.4 (1C, CH, 5′); 122.0 (1C, CH, 5); 124.1 (1C, CH, 3′); 125.1 (1C, CH, 3); 148.1 (1C, C, 4′); 149.0 (1C, CH, 6′); 149.2 (1C, CH, 6); 150.8 (1C, C, 4); 156.0 (1C, C, 2′); 156.3 (1C, C, 2). ^{29}Si NMR δ_{Si}(79.39 MHz; $CDCl_3$; ppm) −45.3 (s, T^0). MS (DCI/NH_3) m/z 403 $(M)^+$. **2** UV δ_{max}(EtOH)/nm 240 (ε dm^3 mol^{-1} cm^{-1} 16 829), 283 (19 168). IR ν, δ/cm^{-1} 3306 ν(NH); 2960 $\nu_{as}(CH_3, CH_2)$; 2857 $\nu_s(CH_3, CH_2)$; 1597, 1556, 1460 $\nu(CC)_{bipy}$; 1377 $\delta(CH_2)$; 1252 ν(SiC); 1071 ν(SiOC); 993 δ(Si–O); 735 $\delta(CH_3, CH_2)$. ^{1}H NMR δ_H(300.13 MHz; $CDCl_3$; ppm) 0.01 (6H, m, CH_3, SiMe); 0.51 (2H, m, CH_2, 11-H); 1.08 (3H, t, J_{AB} = 6, CH_3, 13-H); 1.44 (2H, m, CH_2, 10-H); 2.36 (3H, s, CH_3, 7-H); 2.55 (2H, m, CH_2, 9-H); 3.55 (2H, q, J_{AB} = 6, CH_2, 12-H); 3.78 (2H, s, CH_2, 8-H); 7.04 (1H, d, J_{AB} = 6, CH, 5′-H); 7.22 (1H, d, J_{AB} = 6, CH, 5-H); 8.14 (1H, s, CH, 3′-H); 8.22 (1H, s, CH, 3-H); 8.45 (1H, d, J_{AB} = 6, CH, 6′-H); 8.52 (1H, d, J_{AB} = 6, CH, 6-H). $^{13}C\{^1H\}$ NMR δ_C(75.5; $CDCl_3$; ppm) 0.3 (2C, CH_3, SiMe); 13.8 (1C, CH_2, 11); 18.5 (1C, CH_3, 13); 23.5 (1C, CH_3, 7); 23.8 (1C, CH_2, 10); 51.8 (1C, CH_2, 9); 52.6 (1C, CH_2, 8); 58.2 (1C, CH_2, 12); 120.9 (1C, CH, 3′), 122.0 (1C, CH, 3); 122.9 (1C, CH, 5′); 124.9 (1C, CH, 5); 148.1 (1C, C, 4′); 148.9 (1C, CH, 6′); 149.4 (1C, CH, 6); 150.7 (1C, C, 4), 155.9 (1C, C, 2′); 156.3 (1C, C, 2). ^{29}Si NMR δ_{Si}(79.39 MHz; $CDCl_3$; ppm) 7.6 (s, M^0). MS (DCI/NH_3) m/z 344 $(M+H)^+$.
27 B. P. Sullivan, D. J. Salmon and T. J. Meyer, *Inorg. Chem.*, 1978, **17**, 3334.
28 I. P. Evans, A. Spencer and G. Wilkinson, *J. Chem. Soc., Dalton Trans.*, 1973, 204.
29 B. P. Sullivan, J. M. Calvert and T. J. Meyer, *Inorg. Chem.*, 1980, **19**, 1404.
30 G. F. Strouse, J. R. Schoonover, R. Duesing, S. Boyde, W. E. J. Jones and T. J. Meyer, *Inorg. Chem.*, 1995, **34**, 473.
31 D. Massiot, F. Fayon, M. Capron, I. King, S. Le Calve, B. Alonso, J.-O. Durand, B. Bujoli, Z. Gan and G. Hoatson, *Magn. Reson. Chem.*, 2002, **40**, 70.
32 L. Dudd, M. Hart, D. Ring, E. Sondaz, J. Bonvoisin and Y. Coppel, *Inorg. Chem. Commun.*, 2003, **6**, 1400.
33 R. P. Bagwe, C. Yang, L. R. Hilliard and W. Tan, *Langmuir*, 2004, **20**, 8336.
34 G. S. Caravajal, D. E. Leyden, G. R. Quinting and G. E. Maciel, *Anal. Chem.*, 1988, **60**, 1776.
35 S. de Monredon, A. Pottier, J. Maquet, F. Babonneau and C. Sanchez, *New J. Chem.*, 2006, **30**, 797.
36 A. Juris, V. Balzani, F. Barigelletti, S. Campagna, P. Belser and A. von Zelewsky, *Coord. Chem. Rev.*, 1988, **84**, 85.